Summer 8-13-2015

Entry Flow and Heat Transfer of Laminar and Turbulent Forced Convection of Nanofluids in a Pipe and a Channel

Yihe Huang
Washington University in St Louis

WASHINGTON UNIVERSITY IN ST. LOUIS

School of Engineering and Applied Science

Department of Mechanical Engineering and Materials Science

Thesis Examination Committee:
Ramesh K Agarwal, Chair
Kenneth Jerina
Swami Karunamoorthy

Entry Flow and Heat Transfer of Laminar and Turbulent Forced Convection of Nanofluids in a Pipe and a Channel

by

Yihe Huang

A thesis presented to the School of Engineering and Applied Science
of Washington University in St. Louis in partial fulfillment of the
requirements for the degree of
Master of Science

August 2015

Saint Louis, Missouri

Content

List of Figures

List of Tables

Nomenclature

List of symbols

h	Surface heat transfer coefficient (W m $^{-2}$ K^{-1})
Nu	Nusselt number
D	Hydraulic diameter (m)
Re	Reynolds number
T	Temperature(^{o}C)
x, y	Cartesian coordinates
v	Velocity (m/s)
ρ	Density (Kg m^{-3})
C_p	Specific heat at constant pressure (J kg^{-1} K^{-1})
μ	Dynamic viscosity(Pa s)
k	Thermal conductivity (w m^{-1}K^{-1})
φ	Particle volume fraction
L_e	Entrance length (m)
L_h	Dimensionless entrance length = L_e / D

Subscripts

bf	Base fluid
p	Nanoparticle

nf	Nanofluid
eff	Effective property

Acknowledgments

I would like to express the deepest appreciation to my research advisor Dr. Agarwal for his forward-looking ideas and significant advising. He gave me an opportunity to join the CFD lab when I transferred my major from Material Science to Mechanical Engineering. I could never finish this thesis without his wholehearted guidance.

Thanks to my committee members, Dr. Jerina and Dr. Karunamoorthy, for taking the time to read the thesis and attend its defense.

Also, I would like to thank my CFD lab-mates for their kind encouragement during this research. I would like to especially thank Tim Wray, Xu Han, Guangyu Bao and Junhui Li for useful discussions and help in this research.

In addition, special thanks go to my academic advisor, Dr. David Peters, for helping in the selection of the courses and other academic help.

Finally I would like to thank everyone who has helped me in completing this thesis by providing technical help and encouragement.

Yihe Huang

Washington University in St. Louis
August 2015

Dedicated to my parents

ABSTRACT

Entry Flow and Heat Transfer of Laminar and Turbulent Forced Convection of Nanofluids in a Pipe and a Channel

by

Yihe Huang

Master of Science in Mechanical Engineering

Washington University in St. Louis, 2015

Research Advisor: Professor Ramesh K. Agarwal

This thesis presents a numerical investigation of laminar and turbulent fluid flow and convective heat transfer of nanofluids in the entrance and fully developed regions of flow in a channel and a pipe. In recent years, nanofluids have attracted attention as promising heat transfer fluids in many industrial processes due to their high thermal conductivity. Nanofluids consist of a suspension of nanometer-sized particles of higher thermal conductivity in a liquid such as water. The thermal conductivity of nanoparticles is typically an order-of-magnitude higher than the base liquid, which results in a significant increase in the thermal performance of the nanofluid even with a small percentage of nanoparticles (~4% by volume) in the base liquid. In this study, Al_2O_3, CuO and carbon nanotube (CNT) nanoparticles with the particle concentration ranging from 0 to 4 % by volume suspended in water are considered as nanofluids. Entrance flow field and heat transfer of nanofluids in a channel and pipe are computed using the commercially available software ANSYS FLUENT 14.5. Both constant wall temperature and constant heat flux boundary conditions are considered. An unstructured two-dimensional mesh is generated by the software ICEM. For turbulent flow simulations, two-equation *k*-epsilon, standard *k*-omega and SST *k*-omega models as well as the one-equation Spalart-Allmaras models are employed. The results are validated and compared using the experimental data and other empirical correlations available in the literature. The entrance length of laminar and turbulent flows in a circular pipe and channel are calculated and compared with the established correlations in the literature. The effect of particle concentrations, Reynolds number and type of the nanoparticles on the forced convective heat transfer performance are estimated and discussed in detail. The results show significant improvement in heat transfer

performance of nanofluids, especially the CNT nanofluids, compared to the conventional base fluids.

Chapter 1 Introduction

1.1 Brief Literature Review

1.1.1 Nanofluids and Thermal Conductivity

The term, nanofluids, referring to the fluid with suspended nanometer-sized particles, was first used by Choi [1].Choi showed that by introducing a small amount of nanoparticles to conventional heat transfer liquids, the thermal conductivity can be increased by two times. After that, many researchers investigated this topic (as shown in figure 1.1), aiming at understanding the characteristics and mechanisms of nanofluids and eventually being able to enhance the thermal conductivity. Masuda et al. [3], Lee et al. [4], Xuan and Li [5], and Xuan and Roetzel [6] stated that the thermal conductivity of the suspensions can increase more than 20% with low nanoparticles concentrations. Easeman et al. [7] experimentally showed that the thermal conductivity can be increased by approximately 60% by adding 5% volume of CuO nanoparticles in water as base fluid. Many factors significantly affecting the thermal conductivity are, but not limited to particle size, particle shape, base fluid material temperature, and additives' properties. These factors have been researched in recent years and numerous models have been proposed to take these factors into account depending upon the application. Some of these typical models will be discussed in the following chapters.

The demand for high heat transfer rate is increasing widely nowadays and there has been a broad application of nanofluids as a heat transfer medium. One example of the growing demand is the revolution in microprocessors, which have continually become smaller and more powerful to meet the demand of big data storage and computing. As a result, a faster heat-flow demand has steadily increased over time due to the fact that the thermal management has become the bottleneck of developing high-performance computing units at a relatively small scale. Another application is in automotive industry, where improved heat transfer could lead to smaller heat exchangers for cooling and therefore save space inside the hood of the vehicle [8]. In industry, nanoparticles used in nanofluids to enhance the thermal conductivity have been made out of many different materials, via both the physical synthesis processes and the chemical synthesis processes. Typical physical methods that produce these materials include the mechanical grinding method and the inert-gas-condensation

technique [9]. As to the application of nanofluids, there is a potential application wherever high heat transfer rate may be required. Nevertheless, more work is still needed to meet the requirements of many industrial applications.

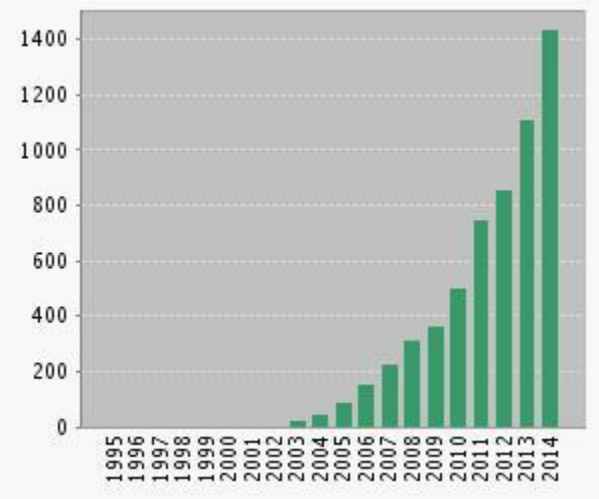

Figure 1.1 Papers related to nanofluids

1.1.2 Entrance Length

In many internal flow applications in industry, entrance length for a conduit is an important parameter among others since it can affect the performance of an industrial component or device. [10]. Generally, the fluid flow in a conduit can be distinguished into two zones: developing flow zone and the fully developed flow zone (as shown in figure 1.2). In the developing flow zone, the boundary layer is not fully developed, while in the fully developed zone the boundary layer is fully developed. The term "entrance length" refers to the distance between the inlet of a conduit and the beginning of the fully developed zone [10]. The entrance length can be affected by many factors, including but not limited to fluid type, conduit material, roughness, cross-sectional area, and angles at the corner of conduit cross-section in some cases [10]. These influences on the entrance length have been studied by many researchers and have been determined using the theoretical, numerical and experimental methods. Simulation tools such as ANSYS Fluent have been widely used as well as other CFD software in numerical simulations.

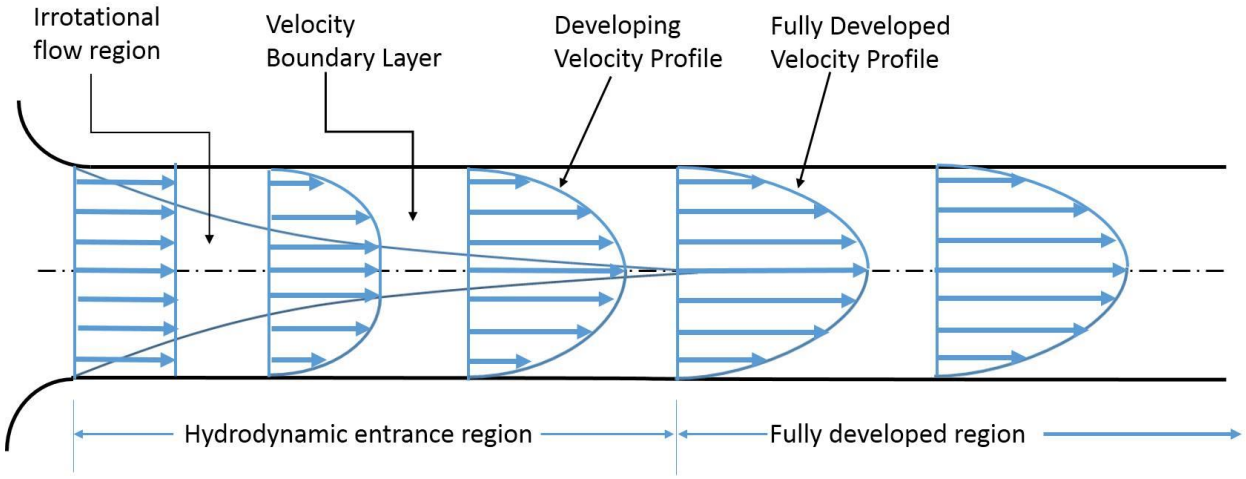

Figure1.2 Fluid flow in a conduit

In industry, the prediction of entrance length is important in quality control and flow management in many cases. One of the apparent examples is the installation position of a flow meter, which is required to provide accurate flow information at the position when flow rate is relatively constant [11]. Additional applications of entrance length estimation are still evolving, which have made the study of entrance length valuable and interesting.

1.2 Overview of Thesis

Due to the potential use of nanofluids as a heat transfer medium with higher thermal conductivity, there is need for better understanding of the heat transfer enhancement properties of various nanofluids. This thesis addresses two problems: one of flow of a nanofluid in a pipe with a constant heat flux boundary condition on the pipe surface and the other is that of channel flow with a constant wall temperature boundary condition; both laminar and fully developed turbulent flow conditions are included. Both the local heat transfer coefficient and the Nusselt number in the entrance region are analyzed. The entrance length of laminar and turbulent flow in a pipe and a channel are numerically calculated and compared with the established correlations in the literature.

Chapter 2 Nanofluids

2.1 Nanofluid Conduction Heat Transfer Properties

2.1.1 Heat Transfer Enhancement Mechanisms

Three mechanisms - Brownian motion, nanoparticles clustering and liquid molecules layering are considered as the three main heat transfer enhancement mechanisms for nanofluids; these mechanisms are briefly described here.

Brownian motion refers to the constant random motion of nano-sized particles suspended in fluid [12-16]. The behavior of these nano-sized particles is very different from the micro- or millimeter-size particles due to the fact that the latter do not move in a stationary base fluid. Therefore, the Brownian motion is an important factor in considering the heat transport from nanofluids. Two mechanisms create Brownian motion in nanofluids [17]: one is due to the collisions among the nanoparticles and the other is the convection induced by random motion of nanoparticles. In some cases, the Brownian motion of nanoparticles can also lead to the aggregation of nanoparticles [18], which may not be desirable in some applications.

Aggregation, which will be referred to as the nanoparticles clustering in this paper, is an inherent property of the nano-particles whether they are suspended in liquid or are in powder form; it results due to van der Waals forces in colloidal suspensions [18]. In order to describe the nanoparticles clustering, numerous models have been developed [19, 20, 21, 22]. These models are widely used nowadays to study the thermal conductivity of different types of nanofluids.

Liquid molecules layering generally refers to the fact that liquid molecules near a solid surface can form layered structures called nanolayers. The nanolayer structure has been recently introduced by Keblinski et al. [19], and Yu and Choi [23] as another mechanism to explain the enhanced thermal conductivity of nanofluids. Figure 2.1 shows the schematic diagram of the basic concept of nanolayers. Nanolayers can be considered as a thermal bridge between a solid particle and a bulk

liquid, which enhances the thermal conductivity. The nanolayer around the particle is assumed to be more ordered than that of the bulk liquid, and the thermal conductivity of the ordered nanolayer k_{layer} is higher than that of the bulk liquid [23].

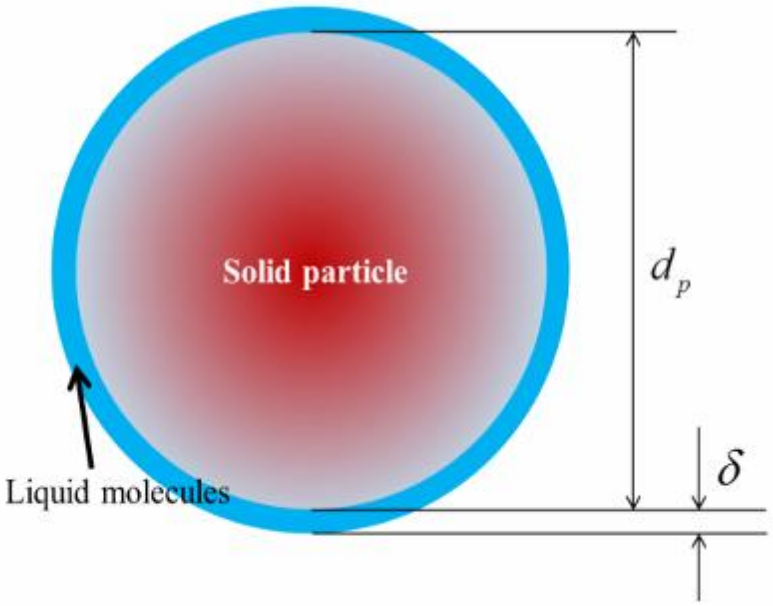

Figure 2.1 Schematic diagram of nanolayers [18]

2.1.2 Models of Nanofluids Thermal Conductivity

The classic Maxwell model [24], proposed by Maxwell in 1904, provides a simple way to calculate the effective thermal conductivity of base fluids with suspended micro particles. In Maxwell model, the effective thermal conductivity of a nanofluid can be computed by the expression:

$$k_{eff} = \frac{k_p + 2k_{bf} + 2\left(k_p - k_{bf}\right)\varphi}{k_p + 2k_{bf} - \left(k_p - k_{bf}\right)\varphi} k_{bf} \tag{2-1}$$

where k_{eff} is the thermal conductivity of the solid-liquid mixture, k_p is the thermal conductivity of the nanoparticle, k_{bf} is the thermal conductivity of the base fluids and φ is the volume fraction of nanoparticles. This model is considered to be good for spherical shaped particles with low particle volume concentrations.

Numerous studies have been conducted after Maxwell to improve upon it for calculating the effective thermal conductivity. In 1962, Hamilton and Crosser [25] extended the Maxwell's model by introducing a factor to take into account the shape of the particle. The thermal conductivity, given by Hamilton and Crosser [25], can be written as:

$$k_{eff} = \frac{k_p + (n-1)k_{bf} - (n-1)\varphi(k_{bf} - k_p)}{k_p + (n-1)k_{bf} + \varphi(k_{bf} - k_p)} k_{bf} \tag{2-2}$$

where n is the empirical shape factor given by $3/\Psi$. Ψ is the particle sphericity, which is defined as the ratio of the surface area of a sphere with the same volume as the particle and the surface area of the non-spherical particle itself.

The above two models and several others of similar type have primarily focused on the micro/millimeter level particles. In order to predict the thermal conductivity of nanofluids, new models and theories have been proposed in the recent years. Among many of the newly developed models, three classes of models have been typically developed: Brownian models, clustering models and liquid layering models. These three models are discussed below.

2.1.2.1 Brownian models

The Brownian motion of the suspended nano-particles is considered to be the most important factor in enhanced thermal conductivity of nanofluids by Chon et al. [26] and many others. Based on this, they proposed an empirical correlation for the thermal conductivity of Al_2O_3 particle based nanofluids from their experimental data using Buckinghan-Pi theorem with a linear regression scheme [26]. The correlation is given as:

$$\frac{k_{nf}}{k_{bf}} = 1 + 64.7\varphi^{0.7460}\left(\frac{d_{bf}}{d_p}\right)^{0.3690}\left(\frac{k_p}{k_{bf}}\right)^{0.7476} \mathrm{Pr}^{0.9955}\,\mathrm{Re}^{1.2321} \tag{2-3}$$

where d_{bf} : molecular diameter of the base fluid,

$\mathrm{Pr} = \dfrac{C_{pbf}\mu_{bf}}{k_{bf}}$: the Prandtl number of the base fluid,

$\mathrm{Re} = \dfrac{(\rho_{bf}\kappa T)}{(3\pi\mu_{bf}^2 l_{bf})}$: the Reynolds number, and

l_{bf} : mean-free path for the base fluid. A constant value of 0.17 for mean free path of base fluid was used in their paper.

Jang and Choi [27] proposed four factors that may contribute to the enhancement of thermal conductivity of the nanofluids: collision among the molecules of the base fluid, thermal diffusion of nanoparticles, collision of nanoparticles among each other due to the Brownian motion and the collision between the base fluid molecules and the nanoparticles by thermally induced fluctuations. Considering these four factors, the effective thermal conductivity of the nanofluid can be written as:

$$k_{nf} = k_{bf}\left(1-\varphi\right) + \beta_1 k_p \varphi + C_1 \frac{d_{bf}}{d_p} k_{bf}\,\mathrm{Re}_{d_p}^2\,\mathrm{Pr}\,\varphi \tag{2-4}$$

where $\beta_1 = 0.01$ is a constant considering the Kapitza resistance per unit area; $C_1 = 18\times10^6$ is a proportionality constant; Pr is the Prandtl number of the base fluid, and the Reynolds number is defined by $\mathrm{Re}_{d_p} = \dfrac{\bar{C}_{R.M.} d_p}{\nu}$ where $\bar{C}_{R.M.} = \dfrac{\kappa T}{3\pi\mu_{bf} d_p l_{bf}}$ is the random motion velocity of a nanoparticle and ν is the kinematic viscosity of the base fluid. As recommend by Jang and Choi [27], for water-based nanofluids the equivalent diameter $d_{bf} = 0.384\,\mathrm{nm}$ and the mean-free path $l_{bf} = 0.738\,\mathrm{nm}$ at a temperature of $300K$.

In 2004, Koo and Kleinstreuer [28] proposed a new thermal conductivity model for nanofluids, which is based on the conventional static part and the significant impact of Brownian motion on the effective thermal conductivity. The effect of particle size, particle volume fraction and temperature dependence, and the type of particle and base fluid combinations are taken into consideration in this model.

$$k_{static} = k_{static} + k_{brownian} \tag{2-5}$$

$$\frac{k_{static}}{k_{bf}} = 1 + \frac{3(\frac{k_p}{k_{bf}} - 1)\varphi}{(\frac{k_p}{k_{bf}} + 2) - (\frac{k_p}{k_{bf}} - 1)\varphi} \tag{2-6}$$

In above formulas, k_{static} is the static thermal conductivity based on the Maxwell's model and the $k_{brownian}$ is the dynamic part which was generated by employing the micro-scale convective heat transfer of a particle's Brownian motion affected by the ambient fluid motion. This enhanced thermal conductivity component was obtained by simulating Stoke's flow around a spherical nano-particle. The thermal conductivity due to Brownian motion [28] was obtained as:

$$k_{brownian} = 5\times10^4 \beta\varphi\rho_{bf} c_{p,bf} \sqrt{\frac{k_b T}{\rho_p d_p}} f(T,\varphi) \tag{2-7}$$

where ρ_{bf}, $c_{p,bf}$ is the density and specific heat capacity of the base fluid, φ is the volume fraction of nano-particles, k_b is the Boltzmann constant and T is the temperature. The two empirical functions β and f introduced by Koo combine the hydrodynamic interaction between the Brownian-motion-induced fluid particles and the temperature effect.

In recent years, the importance of the interfacial thermal resistance R_f between the nanoparticles and the fluids has also been emphasized by many researchers [29, 30]. The thermal interfacial resistance (Kapitza resistance) is believed to exist in the adjacent layers of the two different materials; the thin barrier layer plays a key role in weakening the effective thermal conductivity of the nanoparticles.

In the new correlation for thermal conductivity of nanoparticles proposed in Ref [31], $R_f = 4\times10^8 km^2/W$ is chosen as the thermal interfacial resistance. By introducing R_f, the original k_p in Eq. (2-6) is replaced by a new $k_{p,eff}$ in the form:

$$R_f + \frac{d_p}{k_p} = \frac{d_p}{k_{p,eff}} \tag{2-8}$$

Li [31] also revised the model of Koo and Kleinstreuer [28] by combining the functions β and f into a new function g, which considered the influence of particle diameter, temperature and volume fraction. For different base fluids and different nanoparticles, the function is different. Only water based nanofluids are considered in the present study due to the abundance of experimental data. For Al_2O_3/water and CuO/water nanofluids, the g function can be expressed as:

$$g'(T,\varphi,d_p) = (a_1 + a_2\ln(d_p) + a_3\ln(\varphi) + a_4\ln(\varphi)\ln(d_p) + a_5\ln(d_p)^2)\ln(T) + (a_6 + a_7\ln(d_p) + a_8\ln(\varphi) + a_9\ln(\varphi)\ln(d_p) + a_{10}\ln(d_p)^2) \quad (2\text{-}9)$$

where $\phi \le 0.04, 300K \le T \le 325K$

With the coefficients $a_i, i = 1,2...10$ based on the type of nanoparticle, and with these coefficients, Al_2O_3/water and CuO/water nanofluids have a R_2 of 96% and 98%, respectively [31] (Table can be found in [31]). Thus, the KKL(Koo-Kleinstreuer-Li) correlation can be written as:

$$k_{brownian} = 5\times10^4 \varphi\rho_{bf} c_{p,bf}\sqrt{\frac{k_b T}{\rho_p d_p}}\, g'(T,\varphi,d_p) \quad (2\text{-}10)$$

The viscosity of the nanofluids using the Einstein's equation [32] is given as:

$$\mu_{nf} = \mu_{bf}(1+2.5\varphi) \quad (2\text{-}11)$$

Brinkman [33] proposed a new correlation that extended the Einstein's equation to suspensions with moderate particle volume fraction, typically less than 4%, as:

$$\mu_{static} = \frac{\mu_{bf}}{(1-\varphi)^{2.5}} \quad (2\text{-}12)$$

Koo and Kleinstreuer [28] further investigated the laminar nanofluids flow using the effective nanofluid thermal conductivity model they developed. For the effective viscosity due to micro mixing in suspensions, they proposed

$$\mu_{eff} = \mu_{static} + \mu_{Brownian} = \mu_{static} + \frac{k_{Brownian}}{k_{bf}} \times \frac{\mu_{bf}}{\mathrm{Pr}_{bf}} \quad (2\text{-}13)$$

where μ_{static} is the viscosity of nanofluids, which is the correlation given by Brinkman.

2.1.2.2 Clustering Models

Brownian motion of nanoparticles and their aggregation is considered to be an important factor by Xuan et al. [34] and many others. Xuan et al. proposed a modified correlation for the apparent thermal conductivity of nanofluid, which is the sum of the Maxwell's model and a term due to Brownian motion of the nanoparticles and clusters. It can be written as:

$$k_{nf} = \frac{k_p + 2k_{bf} - 2\left(k_{bf} - k_p\right)\varphi}{k_p + 2k_{bf} + \left(k_{bf} - k_p\right)\varphi} k_{bf} + \frac{\rho_p \varphi C_{P_p}}{2}\sqrt{\frac{\kappa T}{3\pi\mu_{bf} r_c}} \tag{2-14}$$

where r_c is the mean radius of gyration of the cluster and μ_{bf} is the viscosity of base fluid. Upon inspection, it is found that the second term of Eq. (2-12) does not yield the unit of the thermal conductivity (W/m K). Therefore, the equation is not dimensionally homogeneous. In order to satisfy the dimensional homogeneity, the constant coefficient $\left(\frac{1}{2\sqrt{3\pi}}\right)$ should have a unit instead of being dimensionless. The only condition under which the Eq. (2-12) is dimensionally correct is by assigning a unit of $\left(m/\sqrt{s}\right)$ to this constant coefficient, so that the whole term matches the unit of thermal conductivity.

2.1.2.3 Liquid Layering Model

Yu and Choi [23] proposed a modified Maxwell model to include the effect of a nanolayer surrounding the particles by replacing the thermal conductivity of solid particles with the equivalent thermal conductivity of particles k_{pe}. This is based on the effective medium theory and k_{pe} is obtained as:

$$k_{pe} = \frac{\left[2(1-\gamma) + (1+\chi)^3(1+2\gamma)\right]\gamma}{-(1-\gamma) + (1+\chi)^3(1+2\gamma)} k_p \tag{2-15}$$

where $\gamma = k_{layer}/k_p$ is the ratio of nanolayer thermal conductivity to particle thermal conductivity and $\chi = h/r$ is the ratio of the nanolayer thickness to the particle radius. In their study, the nanolayer thickness h and the thermal conductivity k_{layer} are in the range from 1 to 2 nm and $10k_{bp} < k_{layer} < 100k_{bp}$, respectively. Finally the thermal conductivity of the nanofluid is given as:

$$k_{nf} = \frac{k_{pe} + 2k_{bf} + 2\left(k_{pe} - k_{bf}\right)(1+\chi)^3\varphi}{k_{pe} + 2k_{bf} - 2\left(k_{pe} - k_{bf}\right)(1+\chi)^3\varphi} k_{bf} \tag{2-16}$$

In addition, Xue and Xu [35] developed an implicit relation for the effective thermal conductivity of copper oxide/water and copper oxide/EG nanofluids based on a model of nanoparticles with interfacial shells between the surface of the solid particle and the surrounding liquid.

$$\left(1 - \frac{\varphi}{\omega}\right) \times \frac{k_{nf} - k_{bf}}{2k_{nf} + k_{bf}} + \frac{\varphi}{\omega} \frac{\left(k_{nf} - k_2\right)\left(2k_2 + k_p\right) - \omega\left(k_p - k_2\right)\left(2k_2 + k_{nf}\right)}{\left(2k_{nf} + k_2\right)\left(2k_2 + k_p\right) - 2\omega\left(k_p - k_2\right)\left(k_2 - k_{nf}\right)} = 0 \tag{2-17}$$

where $\omega = \left[\frac{r_p}{r_p + t}\right]^3$, in which k_2 is thermal conductivity of the interfacial shell, t represents the thickness of the interfacial shell and r_p the radius of the nano-particle.

2.2 Nanofluid Convection Heat Transfer Properties

2.2.1 Heat Transfer Coefficient and Nusselt Number

The heat transfer coefficient h_{nf} is a function of temperature in classic natural convective heat transfer, and Newton's law can be applied to the function when the temperature changes are relatively small. The heat transfer coefficient is defined for nanofluids by the expression:

$$h_{nf} = \frac{q_w}{T_w - T_b} \tag{2-18}$$

where q_w is the wall heat flux, T_w is wall temperature, and T_b is the bulk temperature of the nanofluid. The Nusselt number is the ratio of convective to conductive heat transfer across the boundary. The larger is the Nusselt number, the more active is the convective heat transfer performance of the fluid flow. Based on h_{nf}, the Nusselt number of nanofluid is defined as:

$$Nu_{nf} = \frac{h_{nf} D}{k_{nf}} \tag{2-19}$$

where D is the characteristic length, k is the thermal conductivity of the fluid. For nanofluids, k_{nf} is usually predicted by the theoretical model or experimental data.

For fully developed laminar flow in circular tubes, the Nusselt number is given as [36]:

$$Nu_{nf} = \begin{cases} 4.36 & \text{for uniform surface heat flux} \\ 3.66 & \text{for uniform surface temperature} \end{cases}$$

For surface fully developed turbulent flow in smooth circular tubes ($\mathrm{Re}_D > 10,000, 0.7 < \mathrm{Pr} < 160, L/D > 10$), the Nusselt number is given as (Dittus Boelter equation)

$$Nu_D = 0.023 \mathrm{Re}_D^{3/4} \mathrm{Pr}^n \tag{2-20}$$

where L is the pipe test section, D is the pipe test section diameter, Re is the Reynolds number and Pr is the Prandtl number. In particular, for cooling of the fluid $n = 0.3$ and for heating of the fluid $n = 0.4$.

The conventional correlation is not suitable for evaluating the Nusselt number of nanofluids, and the proper physical mechanism of heat transfer enhancement has not yet been established. Hence, researchers have proposed various correlations to predict the Nusselt number of nanofluids.

Xuan and Roetzel [37] proposed a general function for the Nusselt number; it is defined as:

$$Nu_{nf} = f[\mathrm{Re}, \mathrm{Pr}, \frac{k_p}{k_{bf}}, \frac{(\rho c_p)_p}{(\rho c_p)_{bf}}], \varphi, \textit{particle size and shape, flow geometry} \quad (2\text{-}21)$$

where Re is the Reynolds number of nanofluid, Pr is the Prandtl number of nanofluid, Pe is the Peclet number and φ is the volume fraction.

Pak and Cho et al. [38] investigated the turbulent friction and convective heat transfer behaviors of dispersed fluids in a circular pipe experimentally. Two metallic oxide particles, γ-Al_2O_3 and TiO_2, with mean diameter of 13 and 27nm, respectively, were used as working fluids. According to their observation, the Nusselt number for fully developed turbulent flow increased corresponding to the increasing volume concentration as well as Reynolds number. However, it was found that the convective heat transfer coefficient of the nanofluids at a volume concentration of 3% was 12% smaller than that of pure water when compared under the condition of constant average velocity. Therefore better selection of particles having higher thermal conductivity and larger size is recommended in order to enhance the heat transfer performance.
The following correlation is suggested for volume concentration of 0-3%, Reynolds and Prandtl numbers of 10^4 to 10^5 and 6.5 – 12.3, respectively:

$$Nu_{nf} = 0.021 \mathrm{Re}_{nf}^{0.8} \mathrm{Pr}_{nf}^{0.5} \quad (2\text{-}22)$$

Li and Xuan [40] investigated the convective heat transfer and flow characteristics of the nanofluid in a tube. Both the convective heat transfer coefficient and friction factor of Cu-water nanofluid for the laminar and turbulent flow are measured. According to the experimental results, the convective

heat transfer coefficient of the base fluid increased remarkably, and the friction factor of the sample nanofluid with the low volume fraction of nanoparticles is almost not changed. Compared with the base fluid, the convective heat transfer coefficient is increased about 60% for the nanofluid with 2.0 % volume of Cu nanoparticles at the same Reynolds number. A new convective heat transfer correlation for a nanofluid suspended with the nanoparticles under single-phase flow assumption has been established for volume concentration of 0-2% and minimum Re of 800:

$$Nu_{nf} = 0.4328(1+11.25\varphi^{0.754} Pe_p^{\ 0.218}) \mathrm{Re}_{nf}^{0.333} \mathrm{Pr}_{nf}^{0.4} \tag{2-23}$$

Xuan and Li [41] also experimentally investigated the convective heat transfer and turbulent flow features of the Cu-H_2O nanofluid in a straight brass tube of inner diameter of 10mm and length of 800mm. By considering the microconvection and microdiffusion effects of the suspended nanoparticles, they proposed a new correlation for turbulent flow of nanofluids in a tube for volume concentration of 0-2% and Reynolds numbers of 1×104 to 2.5 ×104:

$$Nu_{nf} = 0.0059(1+7.6286)\varphi^{0.6886} Pe_p^{\ 0.001}) \mathrm{Re}_{nf}^{0.9238} \mathrm{Pr}_{nf}^{0.4} \tag{2-24}$$

Vajjha et al. [41] carried out experiments for nanofluids with nanoparticles comprised of aluminum oxide, copper oxide and silicon dioxide in 60% ethylene glycol and 40% water by mass. The rheological and the thermophysical properties such as viscosity, density, specific heat and thermal conductivity were measured to develop the heat transfer coefficient correlation from experiments. The following correlation was proposed for the convective heat transfer:

$$Nu_{nf} = 0.065(\mathrm{Re}_{nf}^{0.65} - 60.22)(1+0.0169\varphi^{0.15}) \mathrm{Pr}_{nf}^{0.542} \tag{2-25}$$

Koo and Kleinstreuer [42] investigated steady laminar nanofluid flow in microchannels simulating by two types of fluid, which consisted of copper oxide nanospheres at low volume concentrations in water or in ethylene glycol. The governing equations for the fluid and the wall were solved numerically considering a new model of effective thermal conductivity. In this model, the conventional static part as well as the dynamic part derived from the particle Brownian motion was considered. From the results, the following conclusion were made: use of large high-Prandtl number carrier fluids, nanoparticles at high volume concentrations of about 4% with elevated thermal

conductivities and dielectric constants very close to that of the carrier fluid, microchannels with high aspect ratios and treated channel walls to avoid nanoparticle accumulation should be employed.

In summary, a general correlation for the heat transfer of nanofluid and the physical mechanism of nanofluid flow needs to be developed. A large deviation in predicted values shows the limitation of the current correlations. This may be due to the various influences coming from particle properties, the composition of basic fluid, the hydrodynamic properties and the heat transfer characteristics.

2.2.2 Friction Factor and Pressure Drop

The fiction factor, or also called the Darcy fiction factor [H. P. G. Darcy(1803-1858)] is defined as:

$$f = \Delta p(D/l)/(\rho V^2/2) \tag{2-26}$$

where Δp is the pressure drop, l is the length of the pressure drop test section, ρ is the fluid density and V is the average velocity of the flow. The pressure drop equation for laminar flow in a horizontal pipe can be written as:

$$\Delta p = f\frac{l}{D}\frac{\rho V^2}{2} \tag{2-27}$$

Then, the Darcy friction factor, which is a dimensionless quantity, for laminar flow in a circular pipe ($\mathrm{Re} < 2320$) is given by the formula:

$$f = \frac{64}{\mathrm{Re}} \tag{2-28}$$

where f is the Darcy friction factor and Re is the Reynolds number. By substituting the pressure drop in terms of the wall shear stress, an alternate expression for the friction factor as a dimensionless wall shear stress is obtained:

$$f = \frac{8\tau_w}{\rho V^2} \tag{2-29}$$

where τ_w is the shear stress at the wall.

For turbulent flow, Haaland [43] correlated a form which is easy to calculate from Moody chart, the expression is given by:

$$\frac{1}{\sqrt{f}} = -1.8\log\left[\left(\frac{\varepsilon / D}{3.7}\right)^{1.11} + \frac{6.9}{\mathrm{Re}}\right] \tag{2-30}$$

where ε is the kinematic eddy viscosity of the fluid.

Most experimental results have shown that the pressure drop of the nanofluids is in fairly good agreement with the values predicted from the conventional correlations for base fluid for both laminar and turbulent flows.

Pak and Cho [38] calculated the Darcy friction factors for the dispersed fluids of the volume concentration ranging from 1% to 3%; they matched well with textbook correlations for turbulent flow of a single-phase fluid. Due to increase in the viscosity of the dispersed fluids, there is an additional pumping penalty of approximately 30% at a volume concentration of 3%.

Li and Xuan [39] experimentally showed that the friction factors of the nanofluids coincide well with those of the water in the pressure drop test, which reveals that dilute nanofluids will not cause extra penalty in pumping power. They concluded that the nanofluid with the low volume fraction, with very small particle size, behaves like a pure fluid. Hence, the suspension of nanofluids incurs almost no augmentation in pressure drop. In another paper [40], they showed that the friction factor correlation for the single phase flow (base fluid) can be extended to the dilute nanofluids.

Duangthongsuk and Wongwises [44] showed that the pressure drop of nanofluids was slightly higher than the base fluid and increases with increasing the volume concentrations. A new correlation for friction factor of the nanofluids was proposed:

$$f_{nf} = 0.96\varphi^{0.052}\,\mathrm{Re}_{nf}^{-0.375} \tag{2-31}$$

Vajjha and Das [41] experimentally investigated the Al_2O_3, CuO and SiO_2 nanofluid in a tube under turbulent flow condition. They showed that the pressure loss of nanofluids also increases with an increase in particle volume concentration. The increase of pressure loss of a 10% in Al_2O_3 nanofluid at a Reynolds number of 6700 is about 4.7 times than that of the base fluid. This is due to the

increase in the viscosity of the nanofluid with high nanoparticle concentration. A generalized equation was derived in the following form:

$$f_{nf} = 0.3164\,\mathrm{Re}^{-0.25}\left(\frac{\rho_{nf}}{\rho_{bf}}\right)^{0.797}\left(\frac{\mu_{nf}}{\mu_{bf}}\right)^{0.108} \tag{2-32}$$

where ρ_{nf} is the density of nanofluid, μ_{nf} is the dynamic viscosity of nanofluid, ρ_{bf} and μ_{bf} are the density of base fluid and the dynamic viscosity of base fluid, respectively. This equation is valid in the range $4000 < \mathrm{Re} < 16000$, $0 \le \varphi \le 0.06$ for CuO and SiO_2 nanofluids and $0 \le \varphi \le 0.01$ for the Al_2O_3/water nanofluids.

Li [31] analyzed the thermal performance of nanofluid flow in a trapezoidal microchannel using pure water and CuO/water with volume fractions of 1% and 4%, with the diameter of nanoparticles of 28.6nm. It was found that nanofluids measuredly enhanced the thermal performance of the microchannel mixture flow with a small increase in pumping power. However, the extra pressure drop, or pumping power, decreases the beneficial effects of nanofluids.

Chapter 3 Methodology

CFD is an abbreviation for Computational Fluid Dynamics. It is a branch of fluid mechanics that uses numerical methods and algorithms to solve the governing equations of fluid flow and provides useful information for analysis and design of systems involving fluid flow. CFD based analysis requires computers to perform the calculations. The main advantage of CFD is that it can be used to solve very complex fluid flow problems.

The CFD analysis procedures are generally divided into three steps: pre-processing, simulation and post-processing. During the preprocessing, the geometry of the problem is defined and the volume occupied by the fluid is divided into discrete cells known as the mesh. The simulation step involves discretizing the governing equations on the mesh generated in the first step by employing a suitable numerical algorithm. The discretized equations are then solved on a computer and the values of the flow variables are obtained at the mesh points. In the final post-processing step, the simulation data is analyzed, visualized and used for analysis and design improvement.

3.1 Governing Equations

The governing equations of fluid flow are partial differential equations that describe the conservation of mass, momentum and energy. These equations can be written as:
Continuity equation:

$$\frac{\partial \rho}{\partial t} + \frac{\partial}{\partial x_i}\left(\rho u_i\right) = 0 \tag{3-1}$$

Momentum equation:

$$\frac{\partial}{\partial t}\left(\rho u_i\right) + \frac{\partial}{\partial x_i}\left(\rho u_i u_j\right) = -\frac{\partial p}{\partial x_i} + \frac{\partial \tau_{ij}}{\partial x_i} \tag{3-2}$$

Energy equation:

$$\frac{\partial}{\partial t}\left[\rho\left(h+\frac{1}{2}u_i^{\,2}\right)\right]+\frac{\partial}{\partial x_i}\left[\rho u_j\left(h+\frac{1}{2}u_i^{\,2}\right)\right]=\frac{\partial p}{\partial t}+\frac{\partial}{\partial x_i}\left(u_i\tau_{ij}+\lambda\frac{\partial \tau}{\partial x_j}\right) \tag{3-3}$$

where the stress tensor τ_{ij} and enthalpy h are expressed in the following manner:

$$\tau_{ij}=\mu\left(\frac{\partial u_i}{\partial x_j}+\frac{\partial u_j}{\partial x_i}\right)-\frac{2}{3}\mu\frac{\partial u_i}{\partial x_i}\delta_{ij} \tag{3-4}$$

$$h=C_pT$$

The governing equations are a coupled system of non-linear partial differential equations containing five equations for six unknown flow-field variables u, v, w, p, ρ, and T. The relationship among p, ρ and T is defined by the equation of state for a given liquid or gas, which provides an additional equation.

3.2 Turbulence Models Review

Most of the flows in nature and in industrial systems are generally turbulent flows. Turbulence describes the random and chaotic motion of viscous fluid flow. Turbulent flows are characterized by fluctuating velocity, pressure and temperature fields. These fluctuations result in fluctuation of transport quantities namely the momentum, energy, and species concentration.

Since these fluctuations are of small scale and high frequency, they are computationally too difficult and expensive to simulate directly in practical engineering applications. Therefore, the instantaneous (exact) governing equations described in section 3.1 are generally time-averaged, ensemble-averaged, or otherwise manipulated to remove the resolution of small scales, thereby resulting in a modified set of equations that are computationally less intensive to solve. These equations are called the Reynolds Averaged or Favre Averaged equations. However, these modified equations contain additional unknown variables which need to be modeled. Therefore turbulence models are needed to determine these additional unknown variables in terms of known quantities [45].Some of the widely used industry standard turbulence models are described below.

3.2.1 Spalart-Allmaras Model [46]

The Spalart-Allmaras model is a simple one-equation turbulence model. It solves a transport equation for the kinematic eddy (turbulent) viscosity. It was specifically designed for aerospace applications involving wall-bounded flows and has been shown to give good results for boundary layers subjected to adverse pressure gradients [45].

In Spalart-Allmaras model, the turbulent viscosity μ_t is computed from

$$\mu_t = \rho\tilde{\nu} f_{v1} \tag{3-5}$$

where $\tilde{\nu}$ is the turbulent kinematic viscosity in majority of the flow field except in the near-wall region (dominated by viscous effects), where a viscous damping function f_{v1} is given by $f_{v1} = \dfrac{\chi^3}{\chi^3 + c_{v1}^3}$ where $\chi = \dfrac{\tilde{\nu}}{\nu}$ is employed.

The transport equation for $\tilde{\nu}$ is given by:

$$\frac{\partial}{\partial t}\left(\rho\tilde{\nu}\right) + \frac{\partial}{\partial x_t}\left(\rho\tilde{\nu}u_i\right) = G_v + \frac{1}{\sigma_{\tilde{\nu}}}\left[\frac{\partial}{\partial x_j}\left\{\left(\mu + \rho\tilde{\nu}\right)\frac{\partial\tilde{\nu}}{\partial x_j}\right\} + C_{b2}\rho\left(\frac{\partial\tilde{\nu}}{\partial x_j}\right)\right] - Y_v + S_{\tilde{\nu}} \tag{3-6}$$

where G_v is the production of turbulent viscosity and Y_v is the destruction of turbulent viscosity that occurs in the near-wall region due to wall blocking and viscous damping. $\sigma_{\tilde{\nu}}$ and C_{b2} are constants and ν is the molecular kinematic viscosity. $S_{\tilde{\nu}}$ is a user-defined source term. The turbulent kinetic energy k is not calculated and the last term in Eq. (3-6) is ignored when estimating the Reynolds stresses.

The following wall boundary conditions are used with Spalart-Allmaras model:
At walls, the modified turbulent kinematic viscosity $\tilde{\nu}$ is zero. If the mesh is fine enough to resolve the viscous sub-layer, the wall shear stress is calculated using the laminar stress-strain relationship:

$$\frac{u}{u_\tau} = \frac{\rho u_\tau y}{\mu} \tag{3-7}$$

If the mesh is too coarse and the viscous sub-layer cannot be resolved, it is assumed that the centroid of the wall-adjacent cell falls within the logarithmic region of the boundary layer, and the law-of-the-wall is employed:

$$\frac{u}{u_\tau} = \frac{1}{\kappa} \ln E \left(\frac{\rho u_\tau y}{\mu} \right) \tag{3-8}$$

where u is the velocity parallel to the wall, u_τ is the shear velocity, y is the distance from the wall, κ is the von Karman constant (0.4187), and E is 9.793.

For separated and transitional flows, we employ both the shear-stress transport (SST) k-ω model and the transitional k-kl-ω model. They both have advantages and disadvantages. Developed by Menter [45], the SST k-ω model is more accurate and reliable for a wider class of flows (e.g. adverse pressure gradient flows, transonic flows etc.) than the standard k - ω model.

3.2.2 Shear-stress Transport (SST) k - ω Model [46]

The SST k - ω model effectively blends the robust and accurate formulation of k - ω model in the near-wall region with the k - ε model away from the wall region. To achieve this, the standard k - ω model and the k - ε model are both multiplied by a blending function and both models are then added together. The blending function is used to activate the standard k - ω model in the near-wall region and the k - ε model away from the surface.

The SST k - ω model consists of the following two transport equations for the turbulent kinetic energy (k) and the specific dissipation rate (ω).

$$\frac{\partial}{\partial t}(\rho k) + \frac{\partial}{\partial x_i}(\rho k u_i) = \frac{\partial}{\partial x_j}\left(\Gamma_k \frac{\partial k}{\partial x_j} \right) + \tilde{G}_k - Y_k + S_k \tag{3-9}$$

$$\frac{\partial}{\partial t}(\rho \omega) + \frac{\partial}{\partial x_i}(\rho \omega u_i) = \frac{\partial}{\partial x_j}\left(\Gamma_\omega \frac{\partial \omega}{\partial x_j} \right) + G_\omega - Y_\omega + D_\omega + S_\omega \tag{3-10}$$

where $\tilde{G}_k$ represents the generation of turbulent kinetic energy due to mean velocity gradients. G_ω represents the generation of ω. Γ_k and Γ_ω represent the effective diffusivity of k and ω. Y_k and

Y_ω represent the dissipation of k and ω due to turbulence. D_ω represents the cross-diffusion term. S_k and S_ω are user-defined source terms.

The effective diffusivities are given by:

$$\Gamma_k = \mu + \frac{\mu_t}{\sigma_k} \tag{3-11}$$

$$\Gamma_\omega = \mu + \frac{\mu_t}{\sigma_\omega} \tag{3-12}$$

where σ_k and σ_ω are the turbulent Prandtl numbers for k and ω respectively. The turbulent viscosity μ_t is computed as follows:

$$\mu_t = \frac{\rho k}{\omega} \frac{1}{\max\left[\frac{1}{\alpha^*}, \frac{SF_2}{a_1 \omega}\right]} \tag{3-13}$$

where S is the strain rate magnitude and

$$\sigma_k = \frac{1}{F_1 / \sigma_{k,1} + (1 - F_1) / \sigma_{k,2}} \tag{3-14}$$

$$\sigma_\omega = \frac{1}{F_1 / \sigma_{\omega,1} + (1 - F_1) / \sigma_{\omega,2}} \tag{3-15}$$

α^* damps the turbulent viscosity causing a low-Reynolds-number correction. It's defined by

$$\alpha^* = \alpha_\infty^* \left(\frac{\alpha_0^* + \mathrm{Re}_t / R_k}{1 + \mathrm{Re}_t / R_k} \right)$$

where

$$\mathrm{Re}_t = \frac{\rho k}{\mu \omega} \tag{3-16}$$

$$R_k = 6 \tag{3-17}$$

$$\alpha_0^* = \frac{\beta_i}{3} \tag{3-18}$$

$$\beta_i = 0.072 \tag{3-19}$$

In the high-Reynolds-number form, $\alpha^* = a_\infty^* = 1$. The blending function functions F_1 and F_2 are given by

$$F_1 = \tanh\left(\Phi_1^4\right) \tag{3-20}$$

$$\Phi_1 = \min\left[\max\left(\frac{\sqrt{k}}{0.09\omega y}, \frac{500\mu}{\rho y^2 \omega}\right), \frac{4\rho k}{\sigma_{\omega,2} D_\omega^+ y^2}\right] \tag{3-21}$$

$$D_\omega^+ = \max\left[2\rho \frac{1}{\sigma_{\omega,2}} \frac{1}{\omega} \frac{\partial k}{\partial x_j} \frac{\partial \omega}{\partial x_j}, 10^{-10}\right] \tag{3-22}$$

$$F_2 = \tanh\left(\Phi_2^2\right) \tag{3-23}$$

$$\Phi_2 = \max\left[2\frac{\sqrt{k}}{0.09\omega y}, \frac{500\mu}{\rho y^2 \omega}\right] \tag{3-24}$$

where y is the distance next to the surface and D_ω^+ is the positive portion of the cross-diffusion term.

3.2.3 k-epsilon Model [47]

The $k-\varepsilon$ turbulent transport equations [47] are given as:

$$\rho \frac{\partial k}{\partial t} + \rho U_j \frac{\partial k}{\partial x_j} = \frac{\partial}{\partial x_j}\left(\left(\mu + \frac{\mu_t}{\sigma_k}\right)\frac{\partial k}{\partial x_j}\right) + \tau_{ij} \frac{\partial U_i}{\partial x_j} - \rho\varepsilon \tag{3-25}$$

$$\rho \frac{\partial \varepsilon}{\partial t} + \rho U_j \frac{\partial \varepsilon}{\partial x_j} = \frac{\partial}{\partial x_j}\left(\left(\mu + \frac{\mu_t}{\sigma_\varepsilon}\right)\frac{\partial \varepsilon}{\partial x_j}\right) + C_{1\varepsilon} \frac{\varepsilon}{k} \tau_{ij} \frac{\partial U_i}{\partial x_j} - C_{2\varepsilon} \rho \frac{\varepsilon^2}{k} \tag{3-26}$$

In these equations, $C_{1\varepsilon}$ and $C_{2\varepsilon}$ are constants. σ_k and σ_ε are the turbulent Prandtl numbers for k and ε, respectively and μ_t is the eddy viscosity given by equation

$$\mu_t = \rho C_\mu \frac{k^2}{\varepsilon} \tag{3-27}$$

The various constants in the equations are given in Table 3-1

Table 3.1 Constants used in $k-\varepsilon$ turbulent model

C_μ	$C_{1\varepsilon}$	$C_{2\varepsilon}$	σ_k	σ_ε	σ_t
0.09	1.44	1.92	1.0	1.3	1.0

3.3 Discretization Methods [46]

The governing equations together with boundary and initial conditions are sufficient to obtain a unique solution to the flow field problem. However, the governing equations are partial differential equations with strong non-linearity. They cannot be solved analytically except for some very simple cases. CFD is used to solve the equations in discretized form on a computer.

The approach is to discretize the PDEs into algebraic equations and use suitable iterative numerical methods on a mesh to calculate the solution of the algebraic equations for flow variables. The choice of a suitable numerical algorithm depends on the nature of the governing equation, whether it is hyperbolic, elliptic or parabolic.

In addition, the discretization methods can be classified as finite volume method (FVM), finite element method (FEM), finite difference method (FDM), spectral element method, boundary element method, etc. In our study, we employ the finite-volume method.

The finite volume method (FVM) is the most commonly used approach in majority of CFD codes. It is good at handling issues of memory usage and solution speed, especially for large problems involving high Reynolds number turbulent flows, or source term dominated flows (like in combustion). In the FVM method, the governing partial differential equations - the Navier-Stokes equations, the mass and energy conservation equations, and the turbulence model equations are recast in a conservation form shown in Eq. (3-27). Then they are solved over discrete control volumes (meshes). This guarantees the conservation of fluxes in every cell (control volume). Thus, every equation for a control volume can be written as:

$$\frac{\partial}{\partial t}\int\int\int QdV + \int\int FdA = 0 \tag{3-28}$$

where Q is the vector of conserved variables, F is the flux vector, dV is the volume of the cell, dA is the surface area of the cell.

3.4 Description of ANSYS Fluent

The Navier-Stokes (NS) equations are solved using the commercial code ANSYS FLUENT, a widely used commercial finite-volume method (FVM) based software in computational fluid dynamics (CFD). It is employed to compute the flow properties such as wall shear stress, velocity, temperature, pressure distributions in the flow filed. It is a general-purpose CFD code based on the finite volume method on a collocated grid [45], which is capable of solving steady and unsteady incompressible and compressible, Newtonian and Non-Newtonian flows. FLUENT also provides several zero-, one- and two-equation turbulence models.

ICEM CFD is a pre-processing software used to build geometric models and to generate grids around those models. It allows users either to create their own geometry or to import geometry from most CAD packages. It can also automatically mesh surfaces and volumes while allowing the user to control the mesh through the use of sizing functions and boundary layer meshing. It can generate structured, unstructured and hybrid meshes depending upon the application.

In the current study, the set of governing equations with the associated boundary conditions were numerically solved by finite volume method. The semi-implicit method for pressure-linked equations (SIMPLE) algorithm was used to solve for the pressure and the velocity components. Second order upwind scheme was used to discretize the advective terms in momentum and energy equations to control numerical errors and achieve convergence. The entire domain was initialized with the conditions of inlet boundary before starting the iterative process. In the present analysis, for the constant heat flux boundary condition, axisymmetric flow is considered. For the constant wall temperature boundary condition, planar flow is considered.

Table 3.2 The convergence criteria used for various flow variables and conservation equations

Flow variable	Convergence criteria
Continuity	10^{-6}
x-velocity	10^{-6}
y-velocity	10^{-6}
Energy	10^{-6}

Chapter 4 Entry Flow and Heat Transfer of Laminar Forced Convection of Nanofluids in a Pipe and a Channel

This chapter presents the entrance flow field and heat transfer characteristics of nanofluids in a pipe and a channel. Constant heat flux boundary condition is applied to the pipe flow, and constant wall temperature boundary condition is applied to the channel flow. Water, Al_2O_3/water, CuO/water and CNT/water are used as working fluids. In the current study, various nanofluid materials with different nanoparticle concentrations are used for the forced convection simulations of nanofluids. During the numerical simulations, velocity entrance length, Nusselt number and heat transfer coefficient are calculated.

The mesh generation software ANSYS-ICEM is used to create the geometry and mesh for each model, which is used to create a two- dimensional mesh as an input to the CFD solver ANSYS-FLUENT. To perform the numerical simulations, Fluent is used to calculate the flow field for given flow conditions.

4.1 Computational Modeling

4.1.1 Governing Equations

In our modeling, the nanofluids are treated as continuous and dilute Newtonian mixtures as a single phase fluid. All numerical simulations in this chapter are performed under laminar flow condition. The compression work, dispersion and viscous dissipation are assumed negligible in the energy equation. The conservation equations based on the continuum model of Navier-Stokes equations for a single phase fluid are used to describe the flow flied. These are given in vector notation as follows [47].

The continuity equation can be written as:

$$\nabla \cdot (\rho_{nf} V_m) = 0 \tag{4-1}$$

The momentum or Navier-Stokes equations can be written as:

$$\nabla \cdot (\rho_{nf} V_m V_m) = -\nabla P + \nabla \cdot (\mu_{nf} \nabla V_m) \tag{4-2}$$

The energy equation can be written as:

$$\nabla \cdot (\rho_{nf} C V_m T) = \nabla \cdot (k_{nf} \nabla T) \tag{4-3}$$

The local convective heat transfer coefficient on the wall is given by:

$$h = \frac{-k_{nf} \left. \frac{\partial T}{\partial x} \right|_{wall}}{(T_w - T_b)} \tag{4-4}$$

The local Nusselt number is defined as:

$$Nu = \frac{hD}{k_{eff}} \tag{4-5}$$

The Reynolds number is defined as:

$$\mathrm{Re} = \frac{vD\rho_{nf}}{\mu_{nf}} \tag{4-6}$$

In Equations (4-1)-(4-6), the subscript "*nf* " denotes the nanofluid.

4.1.2 Constant Heat Flux Boundary Condition

The numerical experiments are conducted in an axisymmetric circular pipe. Uniform velocity profile is applied at the inlet of the pipe and pressure outlet boundary condition is used at the outlet boundary, with no-slip boundary condition at the wall. The direction of the flow is from left to right, where in the left boundary is considered as the inlet and the right boundary is considered as the outlet. In order to compare with the experimental study from Kim et al. [48], the diameter of the pipe is set at 0.00457m and the length of the pipe is 4m. During the forced convection simulations, a uniform velocity profile is applied at the inlet and pressure outlet boundary condition is used at the outlet boundary, with no-slip boundary condition at the wall. A constant heat flux of 2089.6 W/m^2 is applied at the wall and an inlet temperature of 295.15k is employed in accordance with the experiments of Kim et al. [47].

Since the variations in the base fluid properties are < 1% in the operating temperature range (295.15K to about 300K), the properties of the solid nanoparticles and base fluids are considered to be constant. The thermophysical properties are listed in Table 4.1

Table 4.1 Thermophysical properties of nanoparticles and base fluid at 295.15K

Properties	Nanoparticles			Base Fluid
	Al_2O_3	CuO	CNT	Water
ρ (Kg m^{-3})	3880	6510	1800	997.7
C_p (J kg^{-1} K^{-1})	729	540	740	4181
k (w $m^{-1}K^{-1}$)	36	76.5	3000	0.6009
μ (Pa s)	-	-	-	0.000958

4.1.3 Constant Wall Temperature Boundary Condition

The numerical experiments are conducted in a two dimensional channel. The width of the channel is at 0.01m and the length of the channel is 4m. A uniform velocity profile is applied at the inlet and the pressure outlet boundary condition is used at the outlet boundary, with no-slip boundary condition at the wall. The direction of the flow is from left to right, with the left boundary being of the inlet and the right boundary as the outlet. A constant wall temperature of 310K and an inlet temperature of 295.15k are employed as boundary conditions.

The thermophysical properties for this case are also taken to be the same as given in Table 4.1.

4.1.4 Nanofluid Properties

The classical single phase fluid model is applied to nanofluids. Thermophysical properties in the governing equations are substituted as those of nanofluids. Nanofluid density is estimated by measuring the volume and weight of the mixtures.

$$\rho_{nf} = \varphi\rho_p + (1-\varphi)\rho_{bf} \tag{4-7}$$

where ρ_{nf} is the density of the nanofluid, ρ_p is the density of the nanoparticles, ρ_{bf} is the density of the base fluid and φ is the volume fraction.

The specific heat of the nanofluid can be obtained by assuming thermal equilibrium between the nanoparticles and the base fluid [49] and can be expressed as:

$$(\rho c_P)_{nf} = (1-\varphi)(\rho c_p)_{bf} + \varphi(\rho c_p)_p \tag{4-8}$$

where c_P is the specific heat of nanoparticles.

The viscosity of Al_2O_3/water and CuO/water nanofluids have been determined by the Vajjha et al. [50] as:

$$\mu_{nf} = \mu_{bf}(T)A\exp(B\varphi) \tag{4-9}$$

The thermal conductivity and the viscosity of CNT/water nanofluids are taken from He et al. [51] as listed in Table 4.3.

Table 4.2 Constants in the viscosity equation for the Al_2O_3 and CuO nanofluids [50]

Nanoparticles	A	B	APS(nm)	Concentration	Temperature(K)
Al_2O_3	0.983	12.959	45	$0<\varphi<0.1$	273<T<363
CuO	0.9197	22.8539	29	$0<\varphi<0.06$	273<T<363

Table 4.3 Properties of CNT/water nanofluids[51]

Nanofluids	Nanoparticles concentration	Viscosity (Pa s)	Thermal Conductivity(W/m K) $k = a + bT + cT^2$		
			a	b	c
CNT/water	0.0384	0.00308	51.88156	-0.35487	6.14×10^{-4}

4.1.4.1 Corcione Model [52]

Most traditional models for predicting the effective thermal conductivity of nanofluids only suitable for nanofluids at room temperature; they become inaccurate when the nanofluids temperature is higher than 20-25℃. Hence, a number of new models based on the Brownian motion of the suspended nanoparticles have been proposed by the researchers. However, these new models show large discrepancies among each other. Besides, most of them include empirical constants of proportionality whose values have been determined based on a limit amount of experimental data. In the current study, Corcione's [52] empirical correlation for thermal conductivity based on a wide variety of experimental data is used.

The experimental data upon which the Corcione's correlation is based are extracted from multiple sources, e.g. Xuan et al.[30] for TiO_2 (27nm) + H_2O; Lee et al. [4] for CuO(23.6nm) + H_2O, CuO(23.6nm) + ethylene glycol(EG), Al_2O_3(38.4nm) + H_2O and Al_2O_3(38.4nm) + ethylene glycol(EG), and Das et al.[53] for CuO(28.6nm) + H_2O, and Al_2O_3(38.4nm) + H_2O. The nanoparticle volume fraction and the nanofluids temperature lie in the range between 0.002 and 0.09, and between 294K and 324K, respectively.

The following mean empirical correlation with a 1.86% standard deviation of error has been developed by regression analysis:

$$\frac{k_{eff}}{k_f} = 1 + 4.4\,\mathrm{Re}^{0.4}\,\mathrm{Pr}^{0.66}\left(\frac{T}{T_{fr}}\right)^{10}\left(\frac{k_s}{k_f}\right)^{0.03}\varphi^{0.66} \tag{4-10}$$

where Re is the particle Reynolds number, Pr is the Prandtl number of the base fluid, T is the nanofluids temperature, T_{fr} is the freezing point of the base liquid, k_s is the thermal conductivity of the solid temperature, and φ is the nanoparticle volume fraction. The Reynolds number is defined as $\mathrm{Re} = (\rho_f u_B d_p)/\mu_f$, where ρ_f is the mass density, μ_f is the dynamic viscosity of the base fluid, u_B is the nanoparticle Brownian velocity and d_p is the nanoparticle diameter. The u_B is calculated as the ratio between d_p and the time required to cover such a distance $\tau_D = \left(d_p\right)^2 / 6D$ [54], in which D is the Einstein diffusion coefficient. The nanoparticle Reynolds number is then given by

$$\mathrm{Re} = \frac{2\rho_f k_b T}{\pi \mu_f{}^2 d_p} \tag{4-11}$$

where $k_b = 1.38066 \times 10^{-23}$ J/K is the Boltzmann's constant. In equations (4-10) and (4-11), all the physical properties are calculated at the nanofluids temperature T .

4.2 Constant Heat Flux Boundary Condition

4.2.1 Numerical Validation

For validating the present numerical results, the axial variations of the local Nusselt number are compared with the experimental data of Kim et al [48]. Excellent agreement can be observed between the computed and experimental results. For the validation of the effective nanofluid properties models, Figure 4.2 shows the computed convective heat transfer coefficient of Al_2O_3 nanofluid with 3% volume fraction and its comparison with the experimental result.

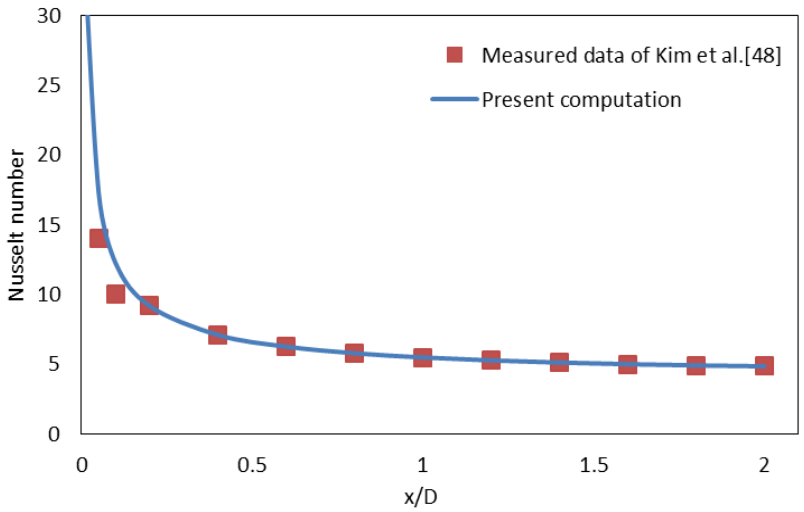

Figure 4.1 Comparison of the computed local Nusselt number with the experimental data for Al_2O_3 nanofluid with 3% volume fraction [48]

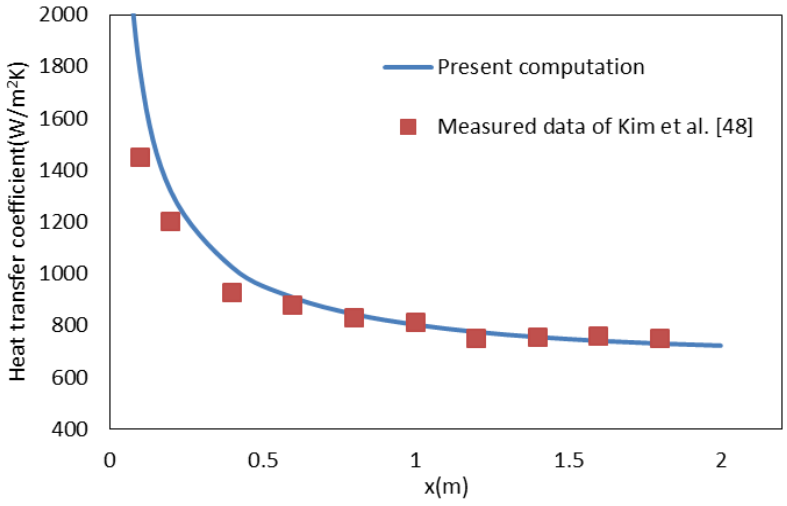

Figure 4.2 Comparison of the computed local heat transfer coefficient with the experimental data for Al_2O_3 nanofluid with 3% volume fraction [48]

4.2.2 Entrance Length Analysis

The distance between the inlet and the fully developed flow zone in a pipe is called the entrance length (L_e); the classic correlations given in Equations (4-12) and (4-13) have been developed to estimate the entrance length of laminar and fully developed turbulent pipe flow, respectively [55].

$$\frac{L_e}{D} \approx 0.06\,\mathrm{Re} \tag{4-12}$$

$$\frac{L_e}{D} \approx 4.4(\mathrm{Re})^{1/6} \tag{4-13}$$

where D is the diameter of the pipe. For the noncircular geometry, the hydraulic diameter can be used instead of the conduit diameter.

The normalized velocity gradient is used in this thesis to determine whether the flow has reached a fully developed status. It is calculated using the equation:

$$\frac{v'(i)}{v(0)} = \frac{[v(i) - v(i-1)]/v(0)}{l_{sample}(i-1,i)/D_h} \tag{4-14}$$

where $v(0)$ is the entrance velocity in m/s, $v(i)$ is the velocity at position i, $l_{sample}(i-1,i)$ is the sampling distance between the i-th sampling point and (i-1)-th sampling point, and D_h is the hydraulic diameter.

Figure 4.3 shows the developing velocity profiles for laminar entry flow in a pipe at Re = 1620 based on its diameter. Figure 4.4 presents the centerline velocity of water and Al_2O_3 nanofluids with different particle concentrations in the circular pipe in axial direction. The centerline velocity increases smoothly near the entrance region, and then reaches a constant value before the outlet. In the present numerical study, the entrance length (L_e) is defined as the distance from the entrance to the point where the centerline velocity reaches 99% or 99.5% of the fully developed value. Table 4.3 gives the dimensionless entrance length value ($L_h = L_e / D$) for 99%, 99.5% and 99.9% of the fully developed value calculated from the numerical simulation. It can be seen from Table 4.3 that the dimensionless entrance length (L_h) of water is 5.66% larger than the value given by Equation (4-12). Furthermore, the L_h value of water is slightly larger than that of Al_2O_3 nanofluids in laminar pipe flow.

Figure 4.5 shows the normalized velocity gradient of water and Al_2O_3 nanofluids with different volume fractions. It is obvious that at the point where L_h is 100, the normalized velocity gradient is nearly 0. Using the numerical results, we obtain a formula with new coefficient for the entrance length for laminar pipe flow:

$$\frac{L_e}{D} \approx 0.063\,\mathrm{Re} \tag{4-15}$$

In equation (4-15), the entrance length is taken as the pipe distance from the entrance to the point where the centerline velocity reaches 99.5% of the fully developed value.

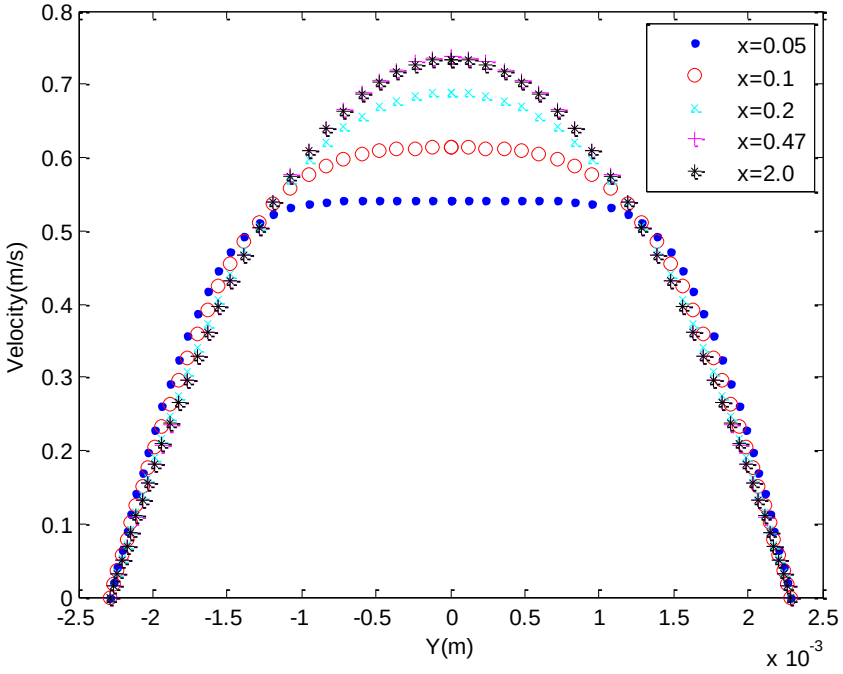

Figure 4.3 Developing velocity profiles for laminar entry flow in a pipe at Re = 1620

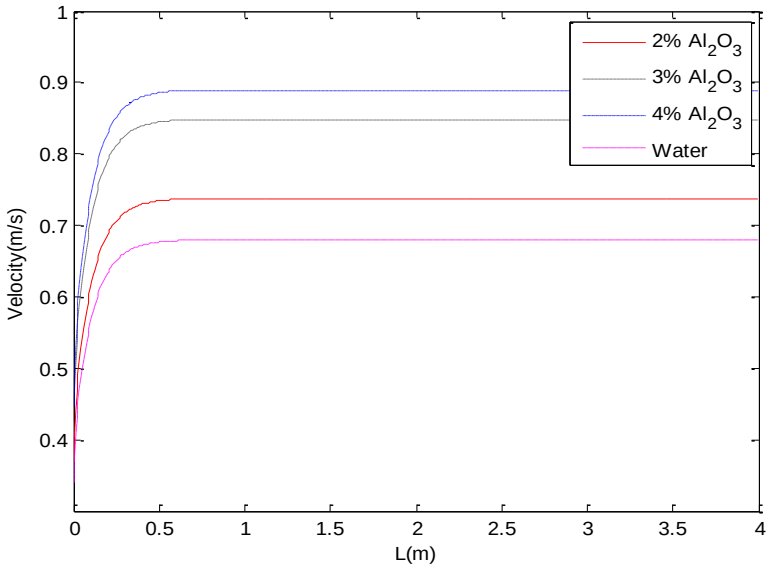

Figure 4.4 Centerline velocity profiles of water and Al_2O_3 nanofluids for laminar pipe flow.

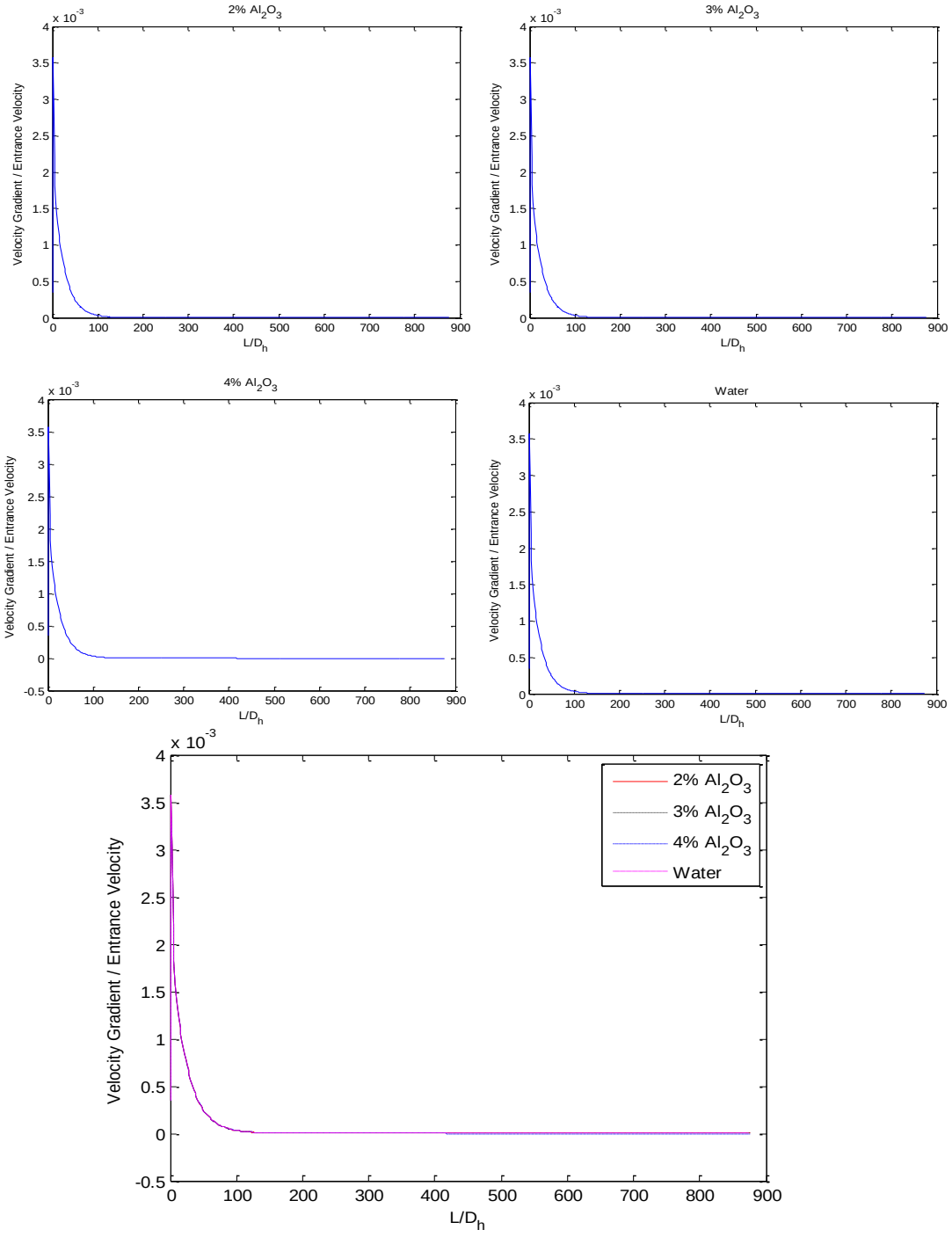

Figure 4.5 The normalized velocity gradient profile of water and Al_2O_3 nanofluids for laminar pipe flow.

Table 4.4 The dimensionless entrance length (L_h) of laminar pipe flow

Working fluid	% of centerline velocity compared to fully developed value			Equation (4-12)
	99%	99.5%	99.9%	
2%Al_2O_3	87.85558	102.5206	127.7611	-
3%Al_2O_3	86.68687	100.4173	122.2689	-
4%Al_2O_3	87.914	102.6374	128.1116	-
Water	87.97243	102.6958	128.2284	97.2

4.2.3 The Effect of Nanoparticle Concentration

For comparisons, pure water, 2% Al_2O_3/water and 4% Al_2O_3/water nanofluids are investigated for the wall and bulk temperature along the axial direction from 0 to 2m. In Figure 4.6, it can be seen that when pure water is a working fluid, it produces higher wall and bulk temperature compared to that from nanofluids. Furthermore, one can also observe that wall and fluid bulk temperature decrease with the augmentation of particle concentrations. This indicates the beneficial effect of better heat transfer properties of nanofluids, which is due to the higher effective thermal conductivity. According to Corcione's model, thermal conductivity of nanofluids increases with increase in nanoparticle volume fraction.

Figure 4.7 shows the effect of particle volume concentration on the heat transfer coefficient along the pipe at Reynolds number 1620. The results show that the heat transfer coefficient increases with the increase in nanoparticle volume concentration. This is due to improvement of convective heat transfer performance with increase in the nanoparticle concentration. At the position where x = 0.6, the heat transfer coefficient of 4% Al_2O_3/water nanofluid increases by 11.2% compared to that of pure water; however, at the position where x = 2.0, the enhancement in heat transfer coefficient goes down to 8.5%. The local Nusselt number along the axial direction shows a similar trend. This

phenomenon indicates that the laminar pipe flow has better heat transfer performance in the entrance region.

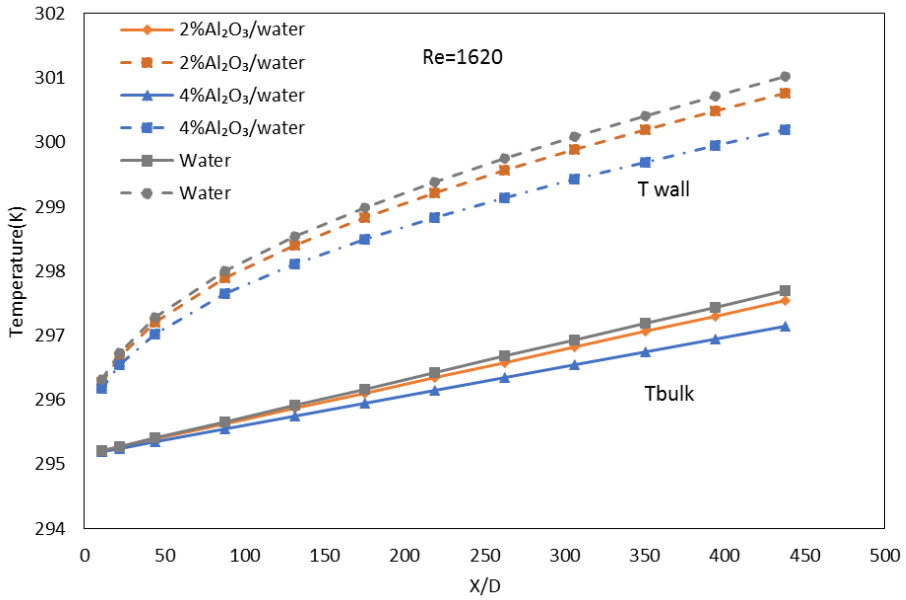

Figure 4.6 Wall and bulk temperature for Water and Al_2O_3 nanofluids in laminar pipe flow at Re = 1620

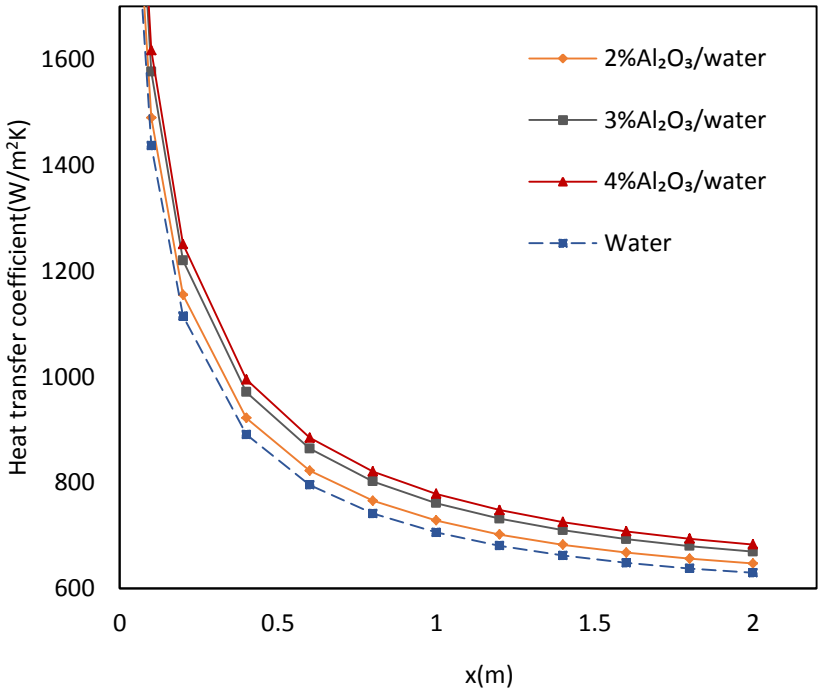

Figure 4.7 Axial variations of heat transfer coefficient for different particle volume concentrations of Al_2O_3/water nanofluid in laminar pipe flow

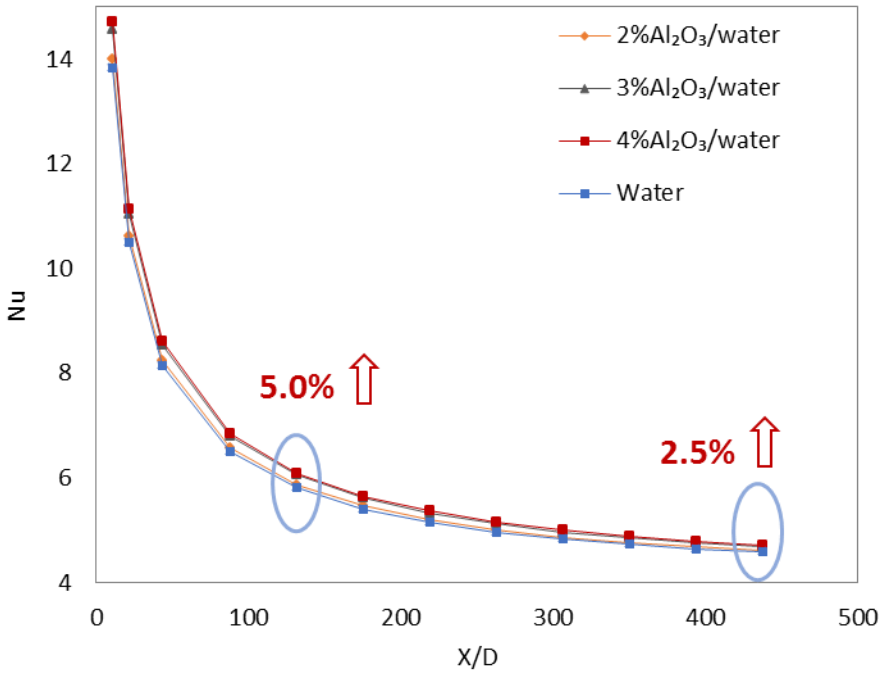

Figure 4.8 Axial variations of Nusselt number for different particle volume concentrations of Al_2O_3/water nanofluid in laminar pipe flow

4.2.4 The Effect of Nanoparticle Material

In order to study the effect of nanoparticle materials in laminar pipe flow; pure water, Al_2O_3/water, CuO/water and CNT/water nanofluids are investigated. Figure 4.9 and Figure 4.10 present comparisons of axial heat transfer coefficient and Nusselt number for nanofluids with different nanoparticles. The results show that the heat transfer coefficient and Nusselt number of CNT/water nanofluid are significantly higher than that of other nanofluids. This may be due to the high aspect ratio surface area of CNT particles compared to other nanoparticles. Also, it can be seen that CuO/water nanofluids give higher convective heat transfer coefficient and Nusselt number than Al_2O_3 nanofluids. This is because the thermal conductivity of CuO nanoparticles is much higher than that of Al_2O_3 nanoparticles

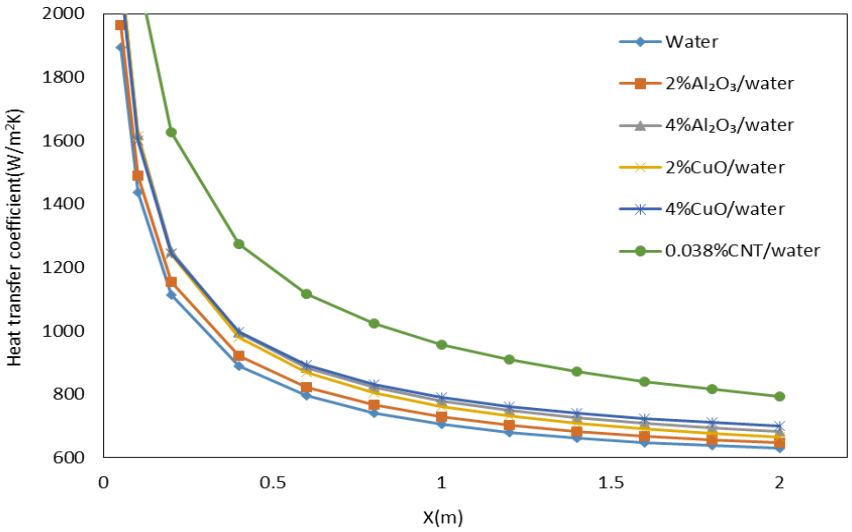

Figure 4.9 Effects of particle type and particle concentration on the local heat transfer coefficient for laminar pipe flow

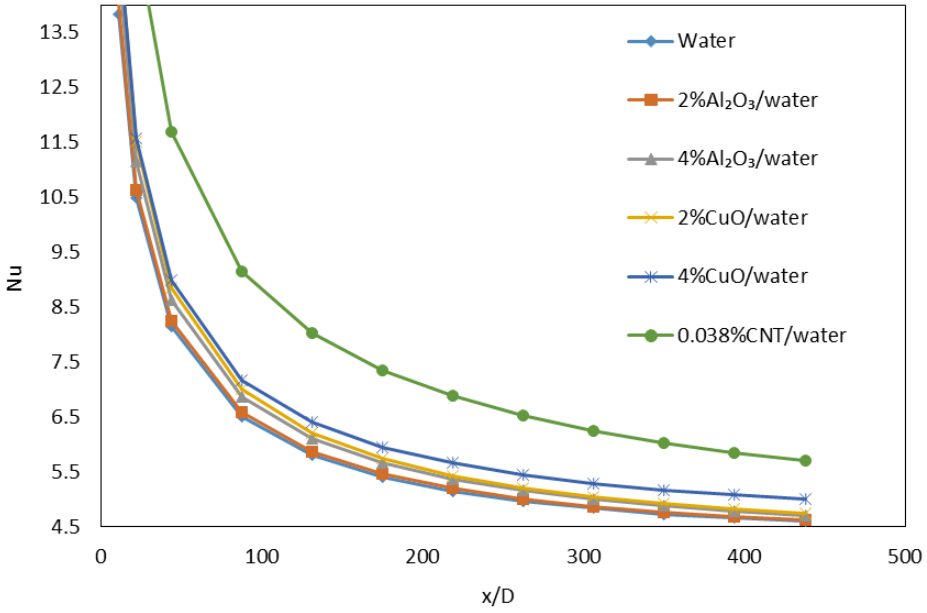

Figure 4.10 Effects of particle type and particle concentration on the local Nusselt number for laminar pipe flow

4.3 Constant Wall Temperature Boundary Condition

4.3.1 Numerical Validation

In order to validate the numerical procedure, the computed results are compared with the classical values in literature [56]. For fully developed laminar channel flow under constant wall temperature boundary condition, the Nusselt number is 7.541. This result was obtained by Etemad (1995) using the finite element solution of the governing conservation equations for Re = 500 and Pr = 10. Figure 4.11 shows the comparison between the local Nusselt number along the axial direction of the channel and the classical value in the fully developed region for a constant wall temperature boundary condition for a channel bounded by two infinite parallel plates. The result agrees well with the theoretical results.

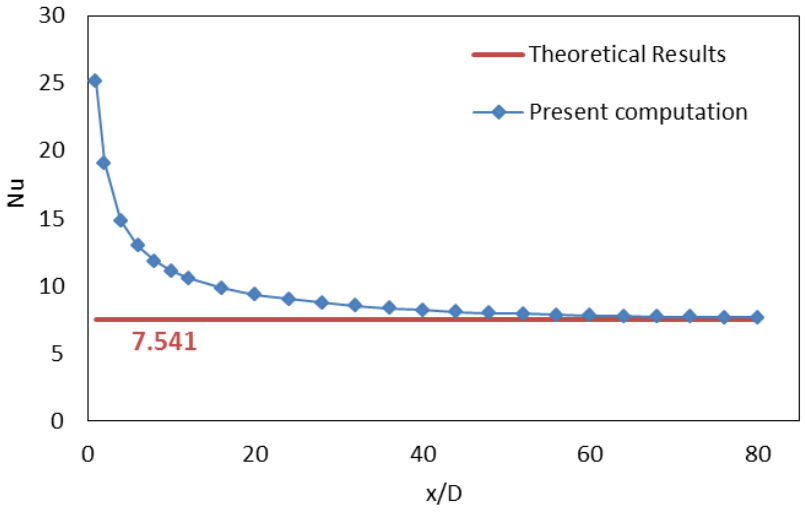

Figure 4.11 Comparison of the axial variations of the computed Nusselt number with the classical result [56] for laminar channel flow of water under constant wall temperature boundary condition

4.3.2 Entrance Length Analysis

J.P.du Plessis and M.R. Collins [57] proposed a definition for laminar flow entrance length of straight ducts. The suggested entrance length is based on hydrodynamic characteristic of the flow development [57]. The entrance length for a channel of width D is given by:

$$Le^{+} = 0.0205 \tag{4-16}$$

$$\text{where } Le^{+} = \frac{L_e}{D\,\mathrm{Re}} \tag{4-17}$$

This L_e^{+} conforms to a 99.77% development of the centerline velocity when applied to the numerical data [57].

Figure 4.12 shows the developing velocity profiles for laminar entry flow in a channel at Re = 500. Figure 4.13 presents the centerline velocity of laminar channel flow in the axial direction at Reynolds number 500. It can be seen that the centerline velocity reaches a fully developed value before the outlet.

Table 4.3 shows the comparison between the L_h value calculated by the current numerical results and the L_h value calculated by Plessis et al. [56]. The entrance length (L_h) of laminar channel flow is calculated at Reynolds number 500.

The L_h value of 9.5456 for water at 99.9% development of centerline velocity is slightly smaller than that calculated using Equation (4-16). From Figure 4.14 it is obvious that the normalized velocity gradient is still much larger than 0 at the point where the L_h value of water reaches 99% of the fully developed value. The normalized velocity gradient nearly reaches 0 when L_h value is larger than 10. In this case, we choose the point where the L_h reaches 99.9% of the fully developed value as the entrance length. According to the numerical results, we obtain a correlation of the entrance length for laminar channel flow as:

$$L_e^{+} = 0.01909 \tag{4-18}$$

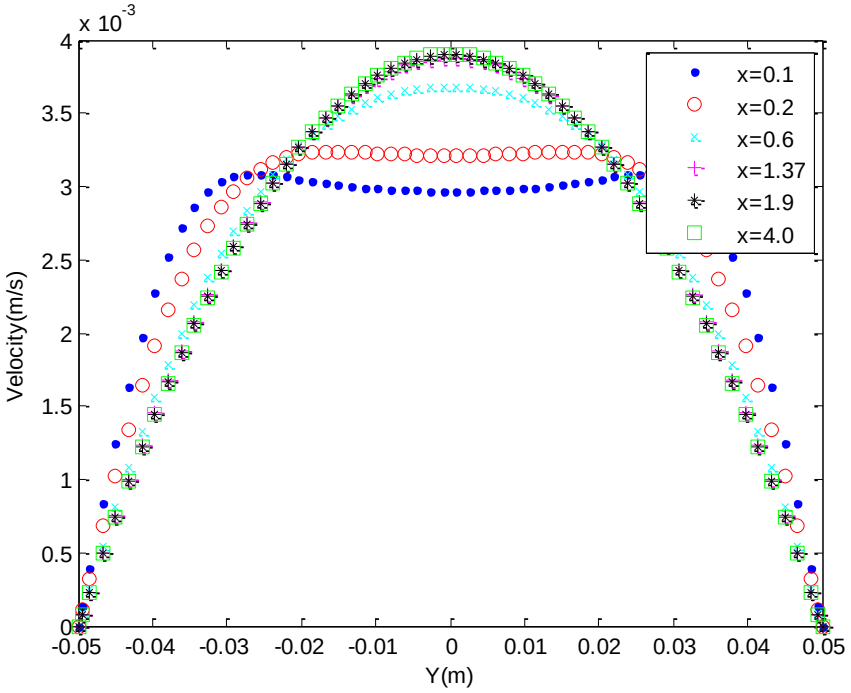

Figure 4.12 Developing velocity profiles for laminar entry flow in a channel at Re = 500

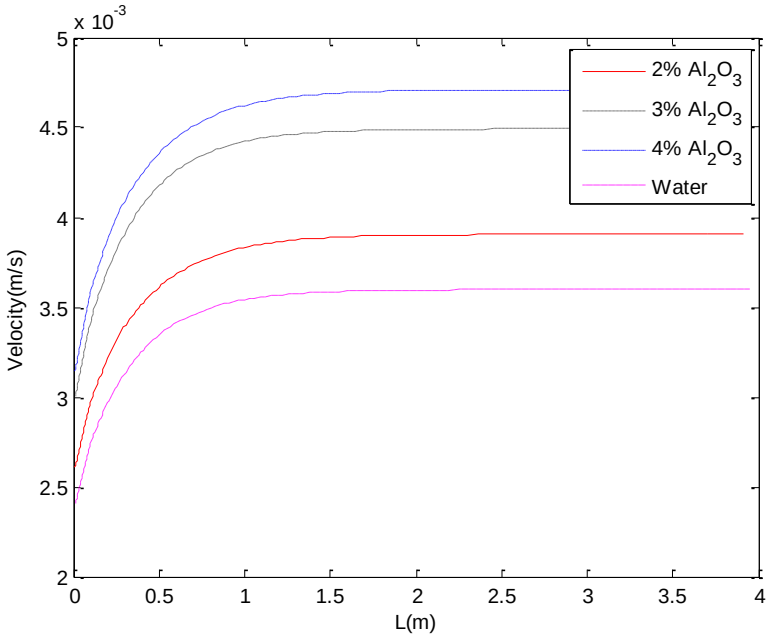

Figure 4.13 Centerline velocity profile of water and Al_2O_3 nanofluids for laminar channel flow at Re = 500

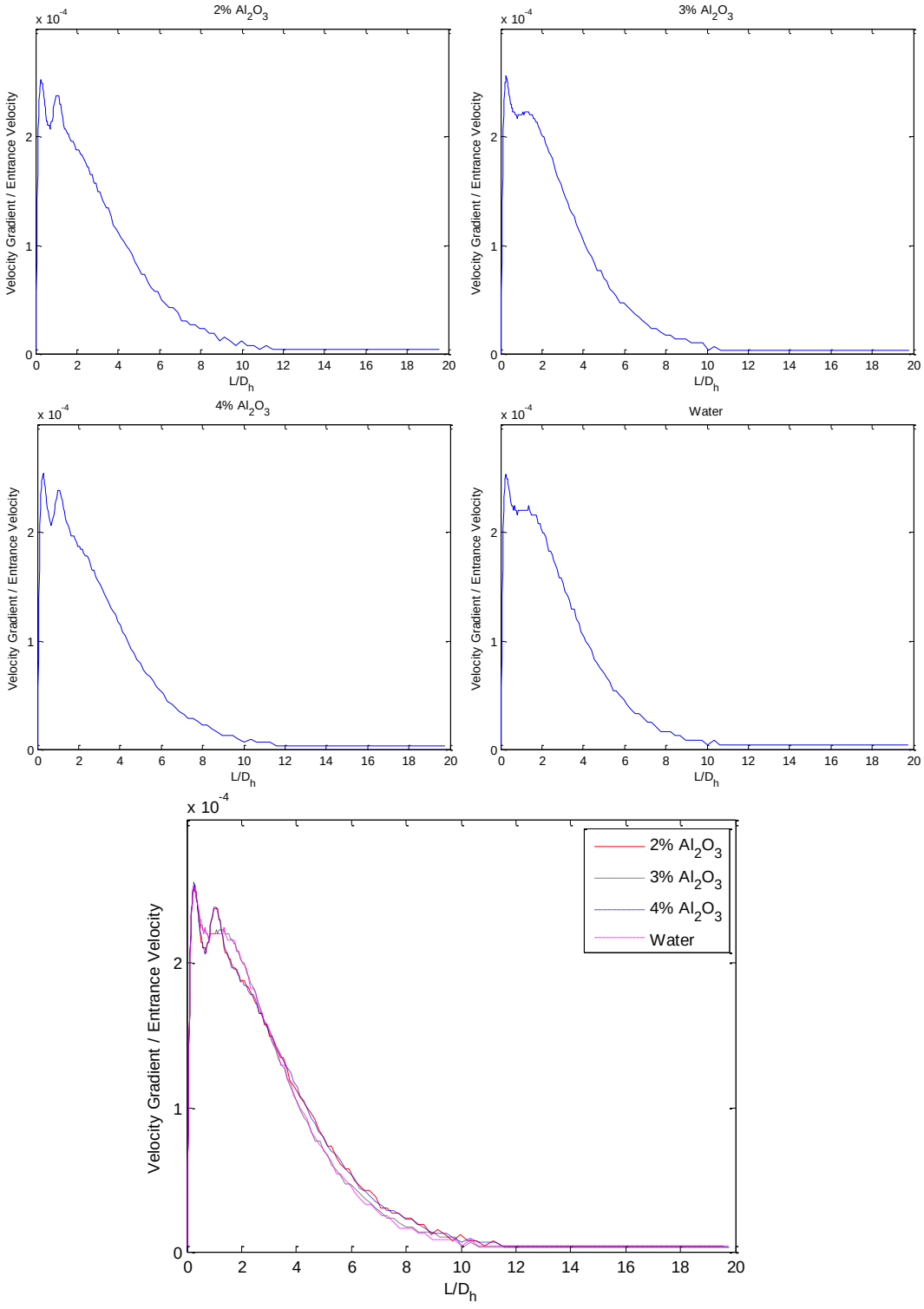

Figure 4.14 The normalized velocity gradient profile of water and Al_2O_3 nanofluids for laminar channel flow

Table 4.5 The dimensionless entrance length (L_h) for laminar channel flow

Working fluid	% of centerline velocity compared to fully developed value			Equation (4-16)
	99%	99.5%	99.9%	
2%Al_2O_3	6.07925	7.30105	10.1086	-
3%Al_2O_3	5.70635	6.85275	9.5456	-
4%Al_2O_3	6.07925	7.30105	10.1086	-
Water	5.70635	6.85275	9.5456	10.25

4.3.3 The Effect of Nanoparticle Concentration

Figure 4.15 represents the effect of volume fraction on the heat transfer coefficient in thermal entrance region of laminar channel flow, Al_2O_3/water nanofluids are used as working fluids. Pure water shows the lowest heat transfer coefficient. It is clear that heat transfer coefficient increases with increase in nanoparticles concentrations. Figure 4.16 illustrates the effect of volume fraction on the local Nusselt number at Reynolds number Re=500. It shows the same trend as the heat transfer coefficient. Al_2O_3/water nanofluid shows the highest Nusselt number, which is caused by the high thermal conductivity of the nanofluid. However, the enhancement in Nusselt number for nanofluids is relatively small: the average Nusselt number in the thermal entrance region of 3%Al_2O_3/water nanofluids increases by 3.60% compared to that for pure water. Also, the laminar channel flow again shows better heat transfer performance in the entrance region when compared to the fully developed region.

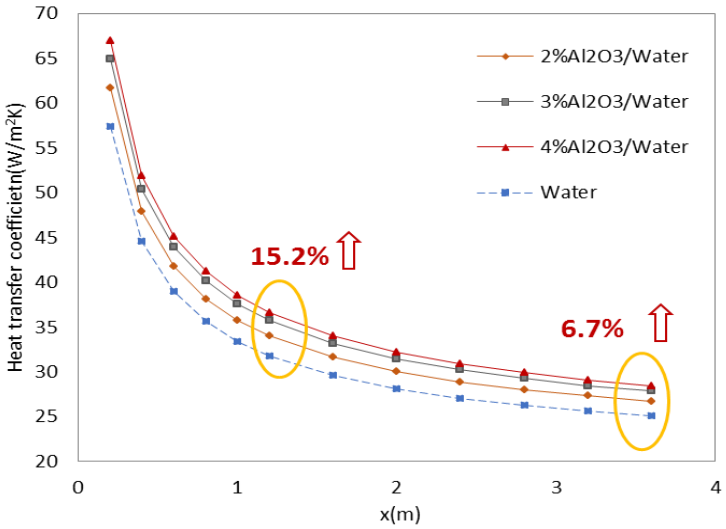

Figure 4.15 Axial variations of heat transfer coefficient for different particle volume concentrations of Al_2O_3/water nanofluid in laminar channel flow

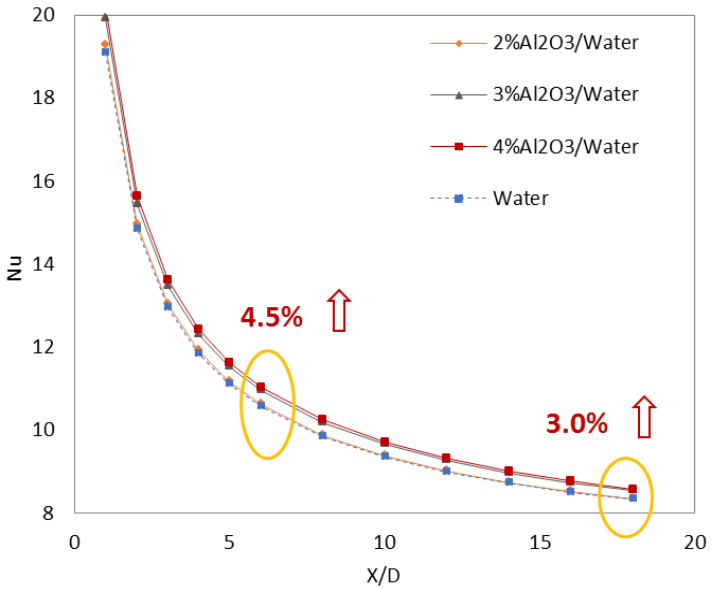

Figure 4.16 Axial variations of Nusselt number for different particle volume concentrations of Al_2O_3/water nanofluid in laminar channel flow

4.3.4 The Effect of Nanoparticle Material

In order to study the effect of nanoparticle materials in laminar channel flow; pure water, Al_2O_3/water, CuO/water and CNT/water nanofluids are investigated. Figure 4.17 and Figure 4.18 present comparisons of axial heat transfer coefficient for nanofluid with different nanoparticles. The results show that the heat transfer coefficient and Nusselt number of CNT/water nanofluids are significantly higher than that of other nanofluids. For CNT/water nanofluids containing 0.038% nanoparticles by volume, the local heat transfer coefficient at position x =2m is 42.53% higher in comparison with the case of pure water, and the local Nusselt number at the same position is 34.6% higher when compared to the case of pure water. Also, it can also be observed that CuO/water nanofluids give higher convective heat transfer coefficient and Nusselt number than the Al_2O_3 nanofluids because of their higher thermal conductivity.

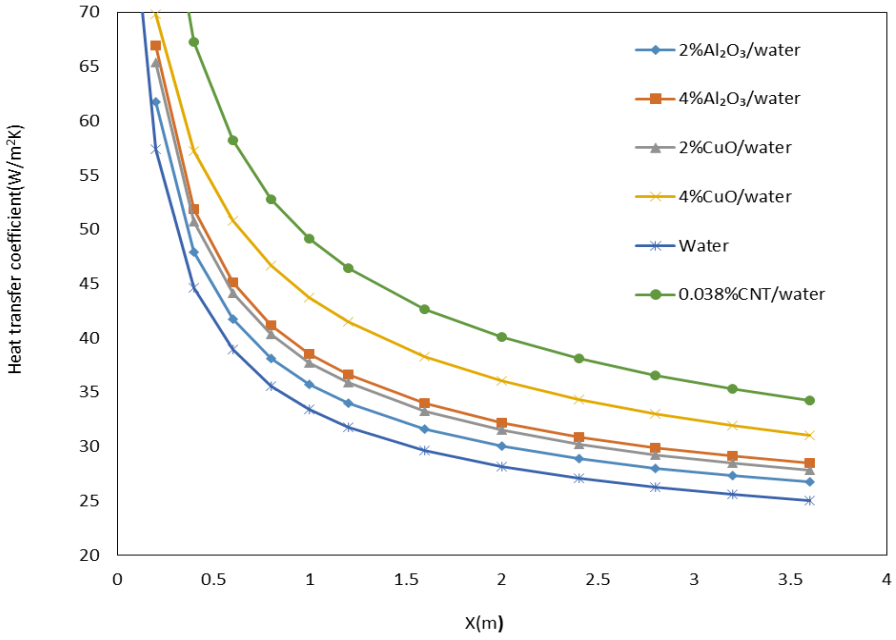

Figure 4.17 Effects of particle type and particle concentration on the local heat transfer coefficient for laminar channel flow

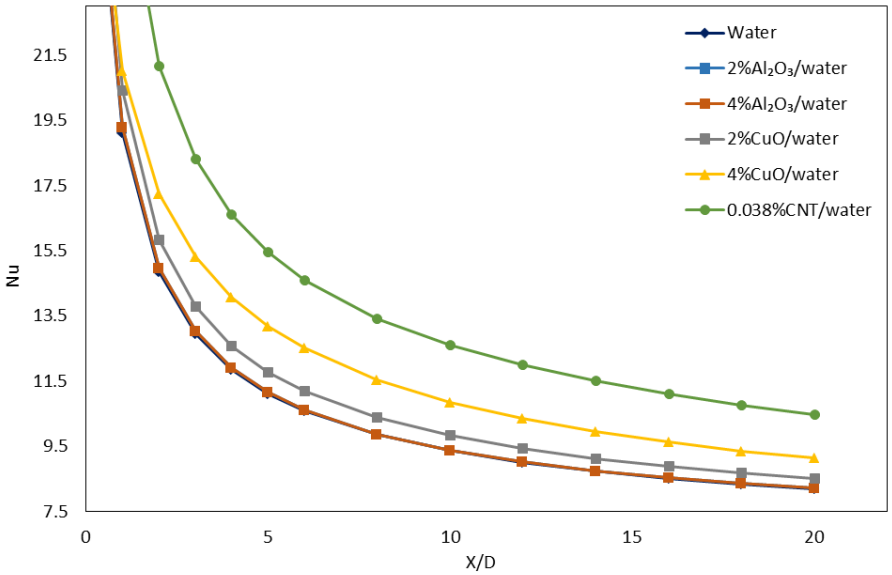

Figure 4.18 Effects of particle type and particle concentration on the local Nusselt number for laminar channel flow

Chapter 5 Entry Flow and Heat Transfer of Turbulent Forced Convection of Nanofluids in a Pipe and a Channel

This chapter presents the turbulent entry flow and heat transfer characteristics of nanofluids in a pipe and a channel. Constant heat flux boundary condition is applied to pipe flow, and constant wall temperature boundary condition is applied to channel flow. Water, Al_2O_3/water, CuO/water and CNT/water are used as working fluids. In this chapter, various nanofluid materials, different nanoparticle concentrations and different Reynolds number are used to study the forced convection of nanofluids via numerical simulation. The velocity entrance length, Nusselt number, and heat transfer coefficient are calculated.

The mesh generation software ANSYS-ICEM is used to create the geometry and the mesh for the pipe and the 2D channel. The mesh is then used as an input to the CFD solver ANSYS-FLUENT. Fluent is used to calculate the flow field for given flow conditions using the RANS equations with a number of turbulence models (k-ε, SST k-ω, k-ω and SA).

5.1 Computational Modeling

5.1.1 Governing Equations

All numerical simulations in this chapter are conducted under turbulent flow condition. As mentioned in Chapter 4, nanofluids are treated as continuous, single phase dilute Newtonian fluid mixtures. The compression work, dispersion and viscous dissipation are assumed negligible in the energy equation. The conservation equations for pipe flow in polar/cylindrical coordinate system (r, z) can be written as follows [58].

The continuity equation is given as [59]:

$$\frac{1}{r}\frac{\partial(rv_r)}{\partial r}+\frac{\partial(v_z)}{\partial z}=0 \tag{5-1}$$

The momentum equations are given as [60]:

$$\frac{1}{r}v_r\frac{\partial(rv_r)}{\partial r}+v_z\frac{\partial v_r}{\partial z}=-\frac{1}{\rho}\frac{\partial p}{\partial r}+(v+v_t)\left[\frac{1}{r}\frac{\partial}{\partial r}\left(\frac{\partial(rv_r)}{\partial r}\right)+\frac{\partial}{\partial z}\left(\frac{\partial(v_z)}{\partial z}\right)\right] \tag{5-2}$$

$$v_z\frac{\partial(v_z)}{\partial z}+\frac{1}{r}v_r\frac{\partial(rv_z)}{\partial z}=-\frac{1}{\rho}\frac{\partial p}{\partial z}+(v+v_t)\left[\frac{1}{r}\frac{\partial}{\partial r}\left(\frac{\partial(rv_r)}{\partial r}\right)+\frac{\partial}{\partial z}\left(\frac{\partial(v_z)}{\partial z}\right)-\frac{v_r}{r^2}\right] \tag{5-3}$$

The energy equation is given as [60]:

$$\frac{1}{r}\frac{\partial(v_rT)}{\partial r}+\frac{\partial(v_zT)}{\partial z}=\frac{1}{r}\frac{\partial}{\partial r}\left(r\alpha_{eff}\frac{\partial T}{\partial r}\right)+\frac{\partial}{\partial z}\left(\alpha_{eff}\frac{\partial T}{\partial z}\right) \tag{5-4}$$

where α_{eff} is the effective thermal diffusivity in SI units, m^2s^{-1}.

The local convective heat transfer coefficient on the wall is given by:

$$h=\frac{-k_{nf}\left.\frac{\partial T}{\partial x}\right|_{wall}}{(T_w-T_b)} \tag{5-5}$$

The local Nusselt number is defined as:

$$Nu=\frac{hD}{k_{eff}} \tag{5-6}$$

The Reynolds number is defined as:

$$\mathrm{Re}=\frac{vD\rho_{nf}}{\mu_{nf}} \tag{5-7}$$

5.1.2 Constant Heat Flux Boundary Condition

For the turbulent flow in a pipe under constant heat flux boundary condition, the same geometry as in chapter 4.1.2 is selected. Uniform velocity profile is applied at the inlet and pressure outlet boundary condition is used at the outlet boundary, with no-slip boundary condition at the wall. The direction of the flow is from the left at the inlet to the right at the outlet. A constant heat flux of 10279.1 W/m^2 at the pipe wall and the inlet temperature of 295.15k are employed based on the experiments of Kim et al. [48]. The turbulent intensity was defined by the formula $I = 0.16\ (Re)^{-1/8}$.

For all the turbulent pipe flow cases considered, the Reynolds numbers based on the diameter is 6020.

The properties of nanofluids considered are the same as given in Chapter 4, as well as the thermophysical properties of solid nanoparticles and base fluids are the same as listed in Table 4.1

5.1.3 Constant Wall Temperature Boundary Condition

Again, the same geometry of a 2D channel as described in Chapter 4.1.3 is selected for the turbulent flow calculations. Uniform velocity profile is applied at the inlet of the channel and the pressure outlet boundary condition is used at the outlet, with no-slip boundary condition at the walls. The direction of the flow is from the left at the inlet to the right at the outlet. A constant wall temperature of 310K and an inlet temperature of 295.15k are employed as boundary conditions.
The properties of the nanofluids considered are the same as given in Chapter 4, as well as the thermophysical properties are taken to be the same as given in Chapter 4.1.1.

5.2 Constant Heat Flux Boundary Condition

5.2.1 Numerical Validation for Pipe Flow

Figure 5.1 shows the y^+ wall value on the axial direction. From Figure 5.1, it can be seen that the dimensionless height y^+ of the first grid cell is less than 1.5, which means that the grid is refined enough in the near-wall region. In order to validate the present CFD solution, the results are compared to the classical correlations and available experimental results in the literature. The Sieder and Tate's correlation [36] is used for the validation; it is given as:

$$Nu_D = 0.027\,\mathrm{Re}_D^{4/5}\,\mathrm{Pr}^{1/3}\left(\frac{\mu}{\mu_s}\right)^{0.14} \tag{5-8}$$

Figure 5.2 shows the comparison between the computed local Nusselt number along the axial direction and the value calculated by Sieder and Tate's correlation. The computed results agree

reasonably well with the correlation given in Equation (5-8). However, the computed results have significant difference with the experimental data of Kim et al. [48].

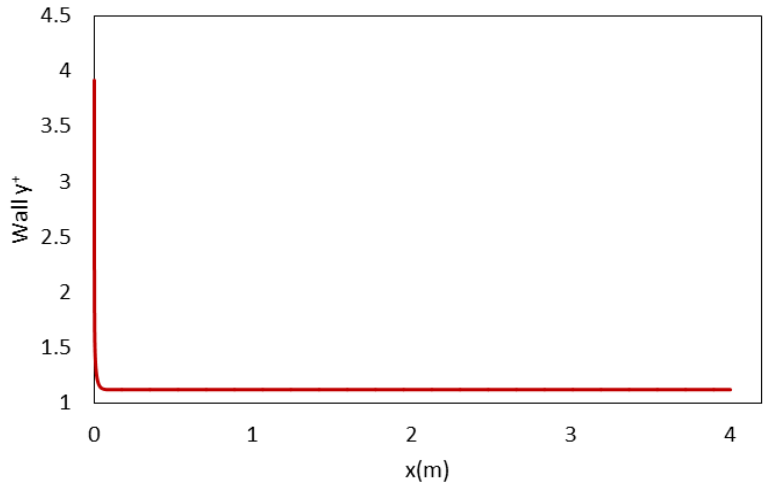

Figure 5.1 The y^+ value at the wall along the axial direction

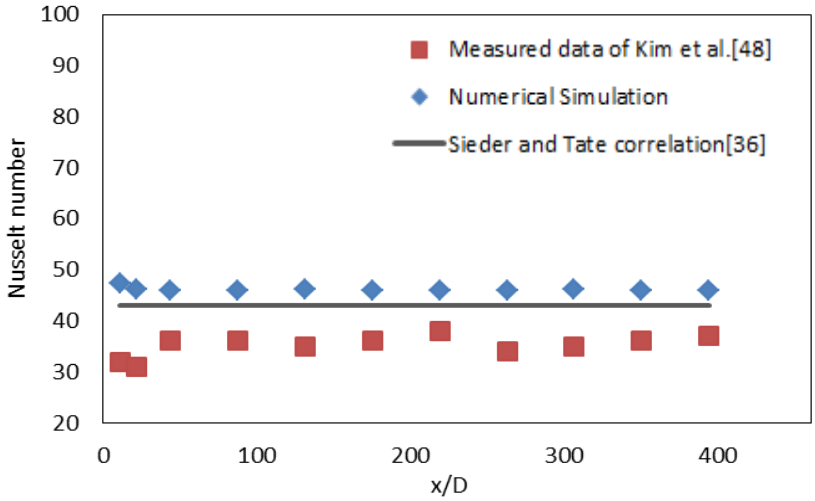

Figure 5.2 Comparison of the axial variation of the Nusselt number with experimental data and the correlation of Sieder and Tate for turbulent pipe flow with constant wall heat flux

5.2.2 Entrance Length Analysis using k-ε Turbulence Model

The entrance length for turbulent pipe flow can be estimated by Equation (4-13) in Chapter 4.2.1. Figure 5.3 shows the developing velocity profiles for turbulent entry flow in a pipe at Re = 6020. Figure 5.4 shows the centerline velocity of water and Al_2O_3 nanofluids with different nanoparticle concentrations in the turbulent pipe flow. It is obvious that the centerline velocity reaches a fully developed value before the outlet. Table 5.1 gives the L_h value for 99%, 99.5% and 99.9% of the fully developed value of the centerline velocity calculated from the numerical simulation. Figure 5.5 shows the normalized velocity gradient of water and Al_2O_3 nanofluids with different particle concentrations.

It can be seen from Figure 5.5 that at the point where the L_h value is 20, the normalized velocity gradient is nearly 0. Hence, we select this point where the L_h value corresponds to 99.9% of the fully developed centerline velocity value as the entrance length. It can be seen that this L_h value is close to that calculated by Equation (4-13). Again, the entrance length of water alone as a fluid is slightly larger than that of the nanofluids. Based on the numerical simulation, we obtain a modified formula with a new coefficient for the entrance length of turbulent pipe flow.

$$\frac{L_e}{D} = 4.28(\mathrm{Re})^{1/6} \tag{5-9}$$

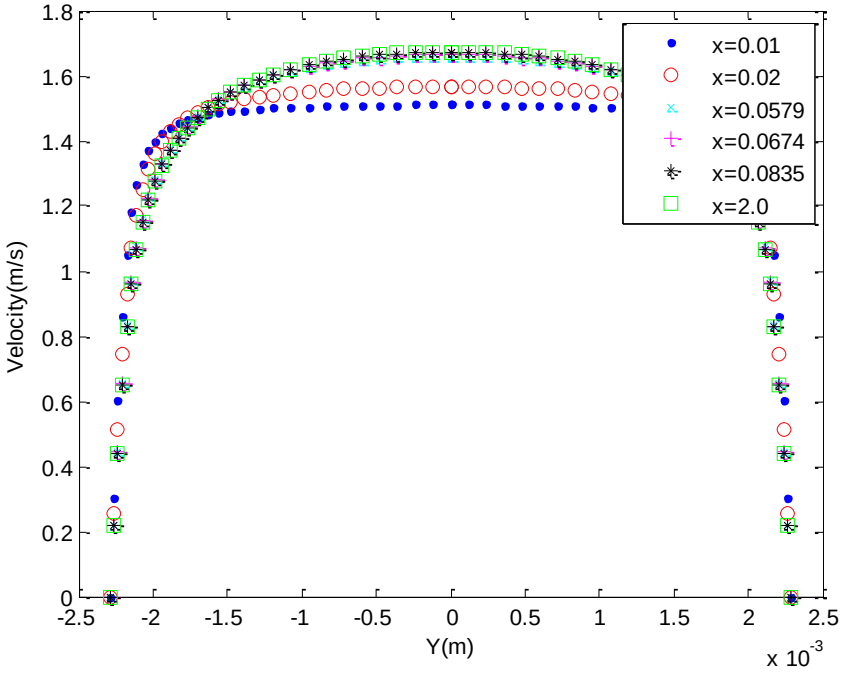

Figure 5.3 Developing velocity profiles for turbulent entry flow in a pipe at Re = 6020 using the k - ε turbulence model

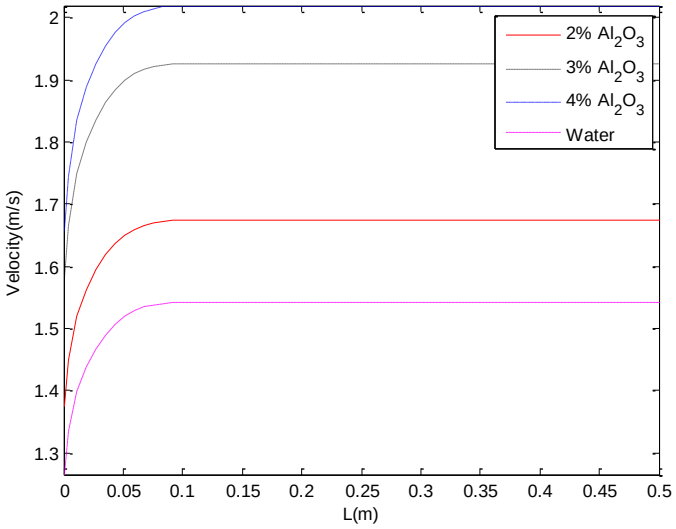

Figure 5.4 Centerline velocity profile of water and Al_2O_3 nanofluids for turbulent pipe flow at Re = 6020 using the k - ε turbulence model

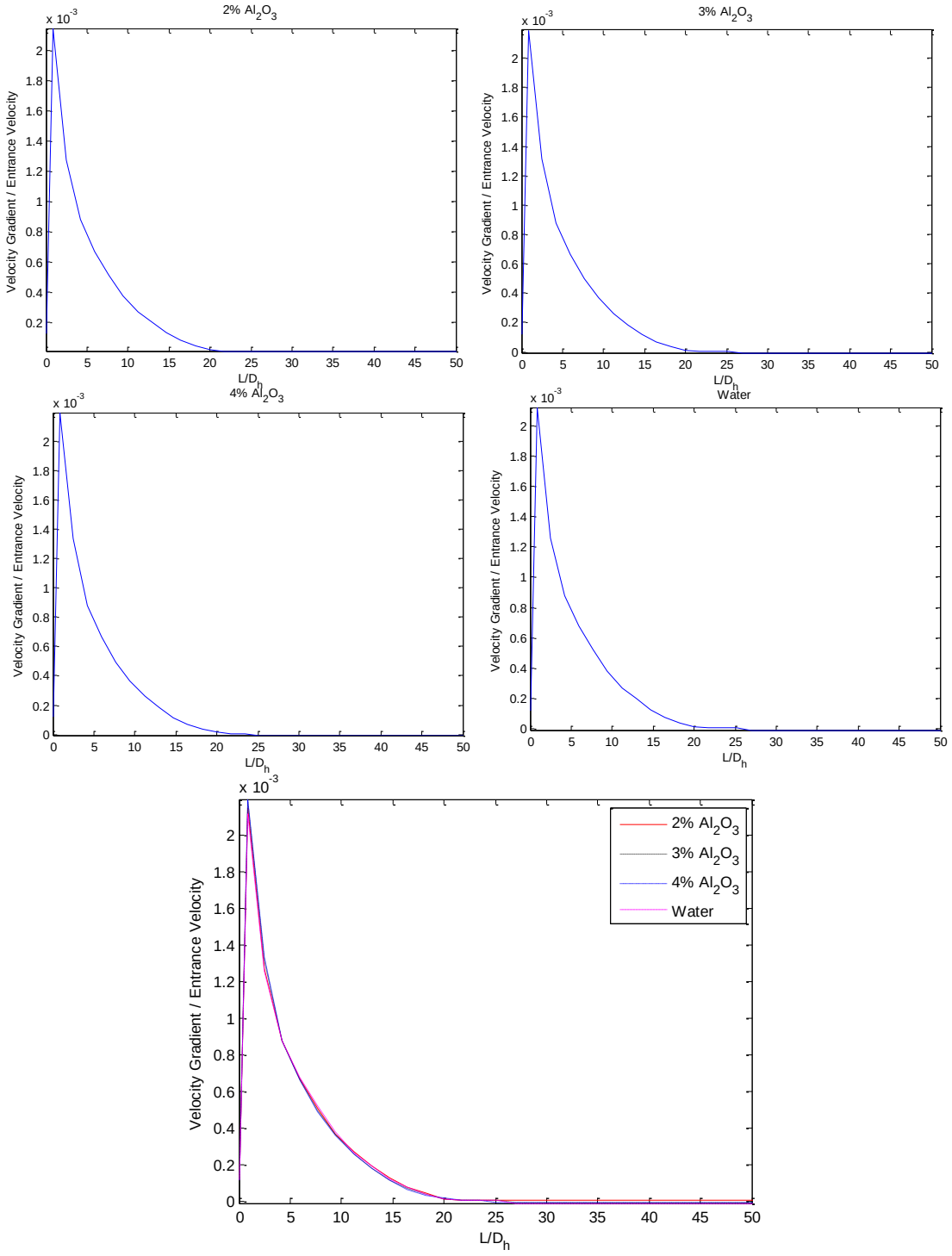

Figure 5.5 The normalized velocity gradient profile of water and Al_2O_3 nanofluids for turbulent pipe flow using the k - ε turbulence model

Table 5.1 The dimensionless entrance length (L_h) of turbulent pipe flow

Working fluid	% of centerline velocity compared to fully developed value			Equation (4-13)
	99%	99.5%	99.9%	
$2\%Al_2O_3$	12.54333	14.6467	18.1523	-
$3\%Al_2O_3$	12.30963	14.41298	17.9186	-
$4\%Al_2O_3$	12.2512	14.35455	17.86018	-
Water	12.66018	14.76354	18.26915	18.766

5.2.3 The Effect of Nanoparticle Concentration

Figure 5.6 shows the effect of particle volume concentration on the heat transfer coefficient along the pipe at Reynolds number of 6020. The results show that the heat transfer coefficient increases with increase in nanoparticle volume concentration. This is due to improvement in convective heat transfer performance with increase in the nanoparticle concentration. Figure 5.7 shows the axial variation of Nusselt number for different particle volume concentrations of Al_2O_3/water nanofluid in turbulent pipe flow. It can be seen that the more Al_2O_3/water nanofluids with 4% particle volume concentrations have the highest Nusselt number as expected. Hence, for turbulent pipe flow at Reynolds number of 6020, the convective heat transfer increases by adding more nanoparticles to the base fluid. As expected, the Nusselt number also reaches an almost constant value before L_h of 20, it implies that the thermal entrance region is smaller for turbulent flow.

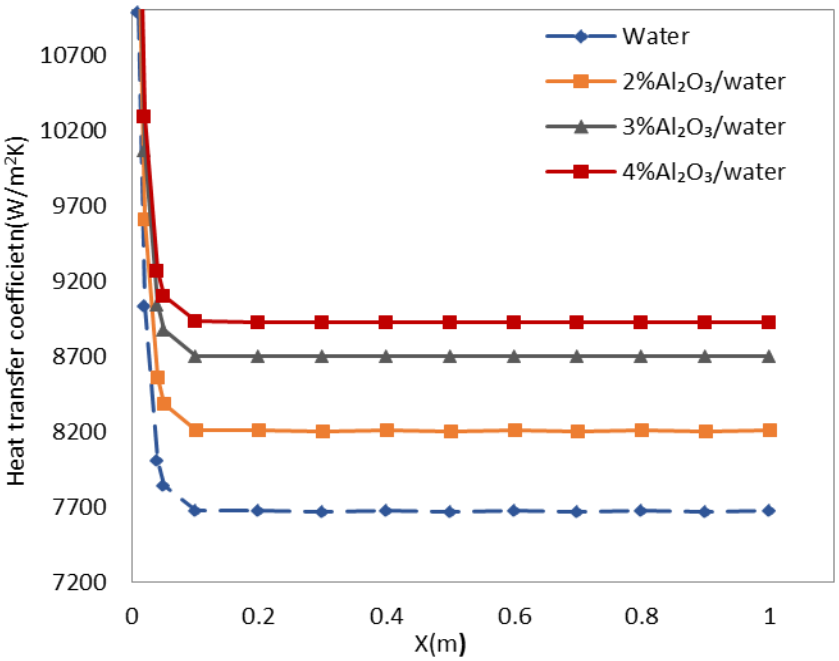

Figure 5.6 Axial variation of heat transfer coefficient for different particle volume concentrations of Al_2O_3/water nanofluid in turbulent pipe flow at Re=6020 using the k - ε turbulence model

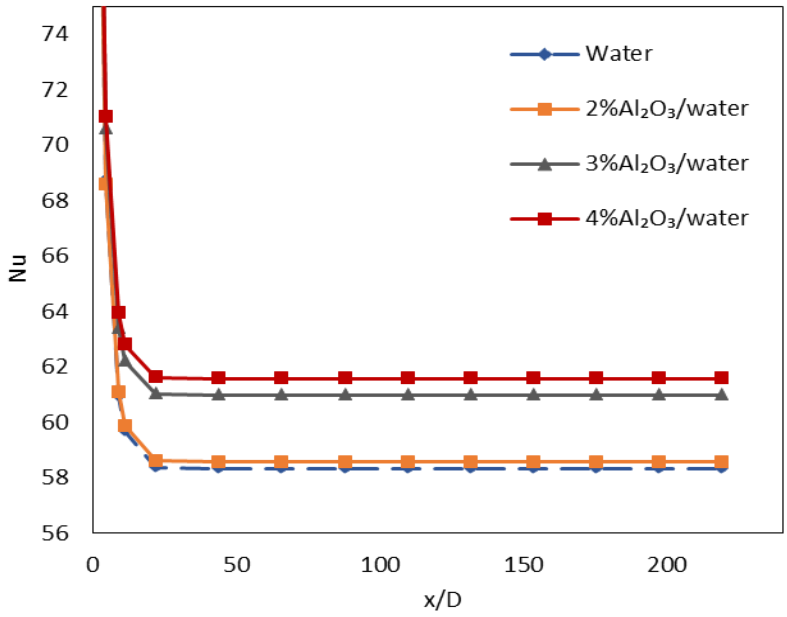

Figure 5.7 Axial variation of Nusselt number for different particle volume concentrations of Al_2O_3/water nanofluid in turbulent pipe flow at Re=6020 using the k - ε turbulence model

5.2.4 The Effect of Nanoparticle Material

In order to study the effect of nanoparticle materials; pure water, Al_2O_3/water and CuO nanofluids with volume fraction 2% and 4% are investigated for turbulent pipe flow at Reynolds number of 6020. In Figures 5.8 and 5.9, it can be seen that CuO/water nanofluids give higher heat transfer coefficient and Nusselt number than the Al_2O_3 nanofluids at the same nanoparticle concentration because of their higher thermal conductivity.

For CuO/water nanofluids with 2% and 4% nanoparticle concentration, the average Nusselt number increases by 7.26% and 19.12% compared to that for pure water, respectively. The average heat transfer coefficient of CuO/water nanofluids with 2% and 4% nanoparticle concentrations increases by 14.38% and 31.61% compared to that for pure water, respectively. This phenomenon indicates that CuO/water nanofluids shows large influence on the convective heat transfer enhancement.

CNT/water nanofluids with small particle concentrations show a significantly higher heat transfer enhancement comparing to the other three nanofluids. For CNT/water nanofluids with 0.038% particle volume fraction, the average heat transfer increases by 51.89% and the average Nusselt number increases by 43.47% compared to that for pure water, respectively.

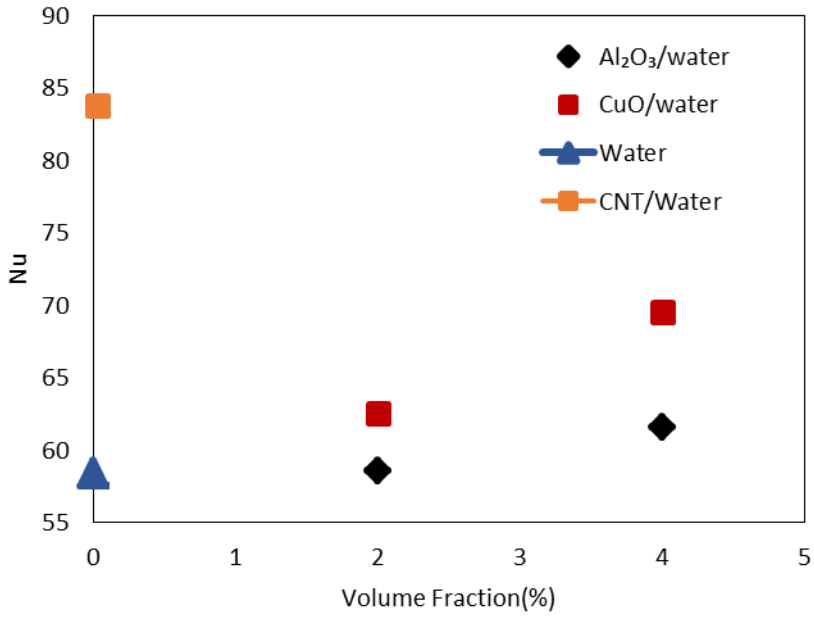

Figure 5.8 Effects of particle type and particle concentration on the average heat transfer coefficient for turbulent pipe flow at Re=6020 using the k - ε turbulence model

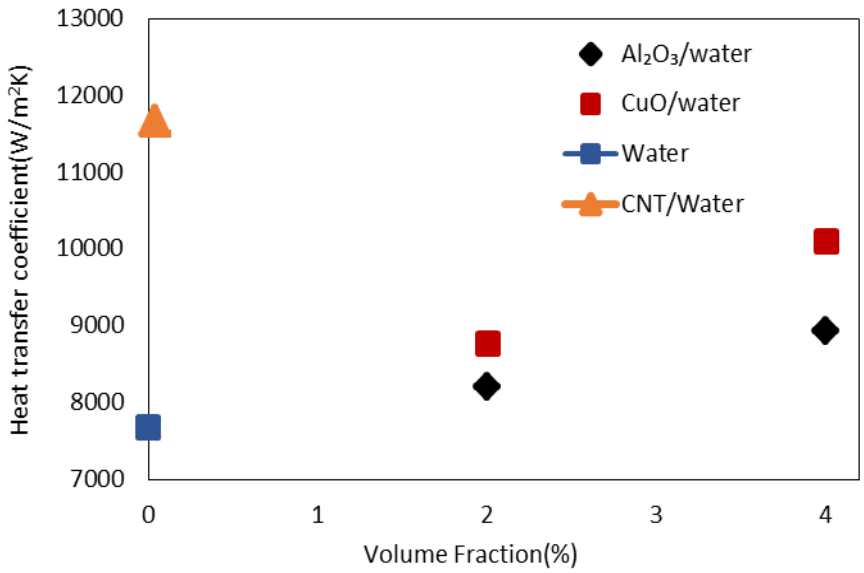

Figure 5.9 Effects of particle type and particle concentration on the average Nusselt number for turbulent pipe flow at Re=6020 using the k - ε turbulence model

5.3 Constant Wall Temperature Boundary Condition

5.3.1 Numerical Validation for Channel Flow

Figure 5.10 shows the y^+ value at the wall along the axial direction. From Figure 5.10, it can be seen that the dimensionless y^+ height of the first grid cell is less than 1, which means that the grid is refined enough in the near-wall region. In order to validate the CFD solution, the computed results are compared with the unpublished results from Kruskopf et al. [61]. Figure 5.11 shows the comparison between the computed fully developed velocity profile from the present study and that from Kruskopf et al. Figure 5.12 shows the friction factor as a function of the Reynolds number for fully developed turbulent channel flow. The computed results in current study are compared with the results of Kruskopf et al. and the values for a smooth-wall turbulent channel flow obtained from White [62]. The present results agree well with the results of Kruskopf et al. and White.

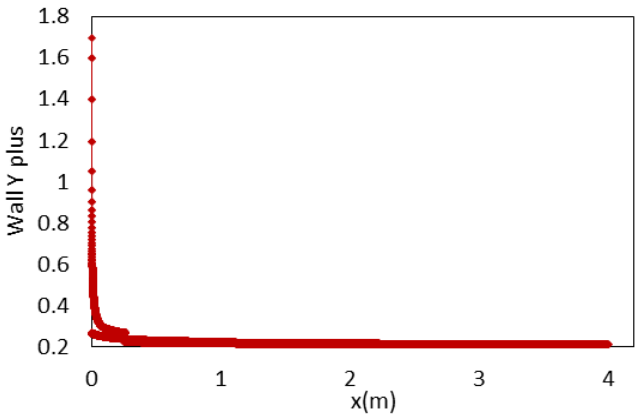

Figure 5.10 The y^+ value at the wall along the axial direction for turbulent channel flow at Re=30,000 using the k - ε turbulence model

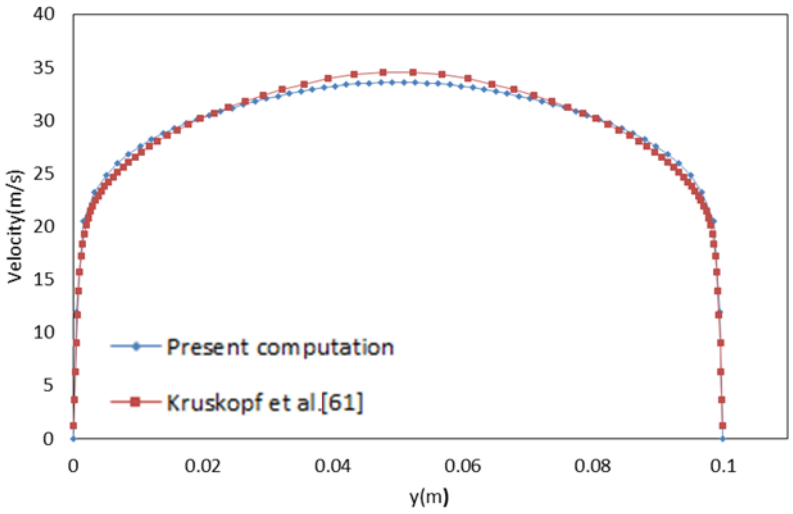

Figure 5.11 Comparison of the fully developed velocity profile for turbulent flow in a channel at Re = 30000 using the k - ε turbulence model

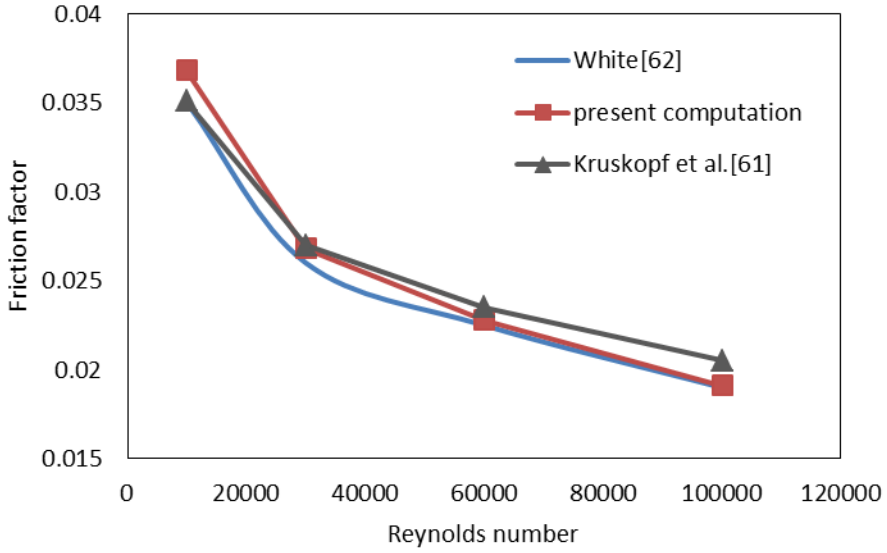

Figure 5.12 Comparison of friction factor for fully developed turbulent flow using the k - ε turbulence model

5.3.2 Entrance Length Analysis using k-ε Turbulence Model

Figure 5.13 shows the developing velocity profiles for turbulent entry flow in a channel at high Reynolds number Re = 30000. Figure 5.14 shows the centerline velocity of water and Al_2O_3 nanofluids with different nanoparticle concentrations in the turbulent channel flow. It can be seen that the centerline velocity reaches an almost fully developed value before the outlet. Table 5.2 gives the L_h value when the centerline velocity achieves 99%, 99.5% and 99.9% of the fully developed value calculated from the numerical simulation. Figure 5.15 shows the normalized velocity gradient of water and Al_2O_3 nanofluids with different particle concentrations in turbulent channel flow.

It can be seen from Figure 5.15 that at the location when the L_h value is 10, the normalized velocity gradient reaches a value near zero. Hence, we select the L_h value when the centerline velocity reaches 99.9% of the fully developed value as the entrance length. Again, the entrance length for flow of pure water is slightly larger than that for flow of nanofluids.

Figure 5.16 shows the centerline velocity profile of water and Al_2O_3 nanofluids for turbulent channel flow at Re = 20000, 30000, 50000. Figure 5.17 presents the normalized velocity gradient profile of water for different Reynolds number for turbulent channel flow. From Figure 5.17, it can be seen that higher Reynolds number results in larger entrance length.

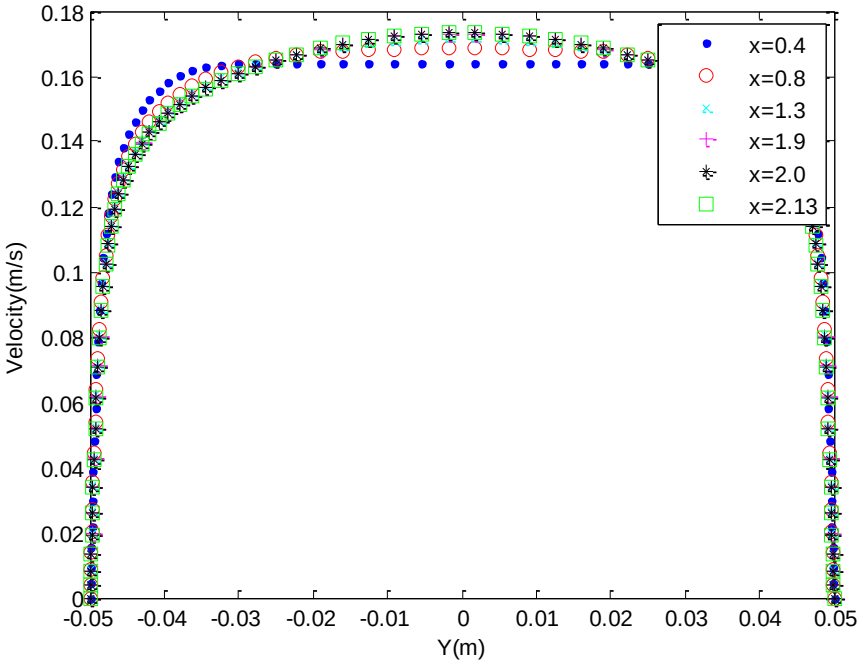

Figure 5.13 Developing velocity profiles for turbulent entry flow in a channel at Re = 30000 using the k - ε turbulence model

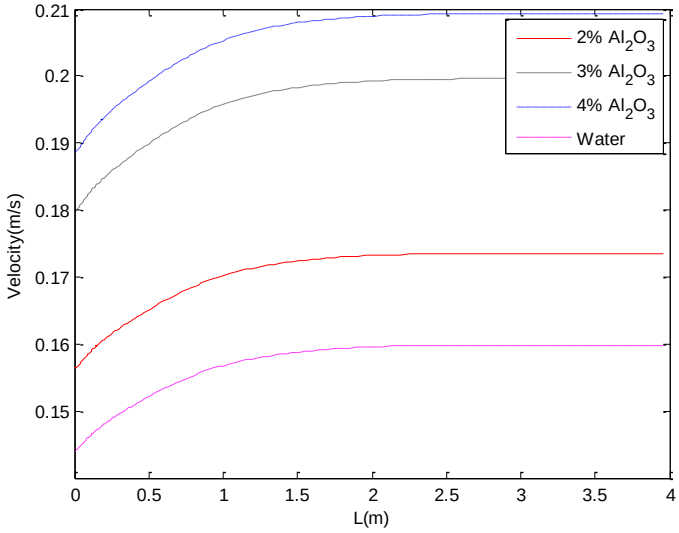

Figure 5.14 Centerline velocity profile of water and Al_2O_3 nanofluids for turbulent channel flow at Re = 30000 using the k - ε turbulence model

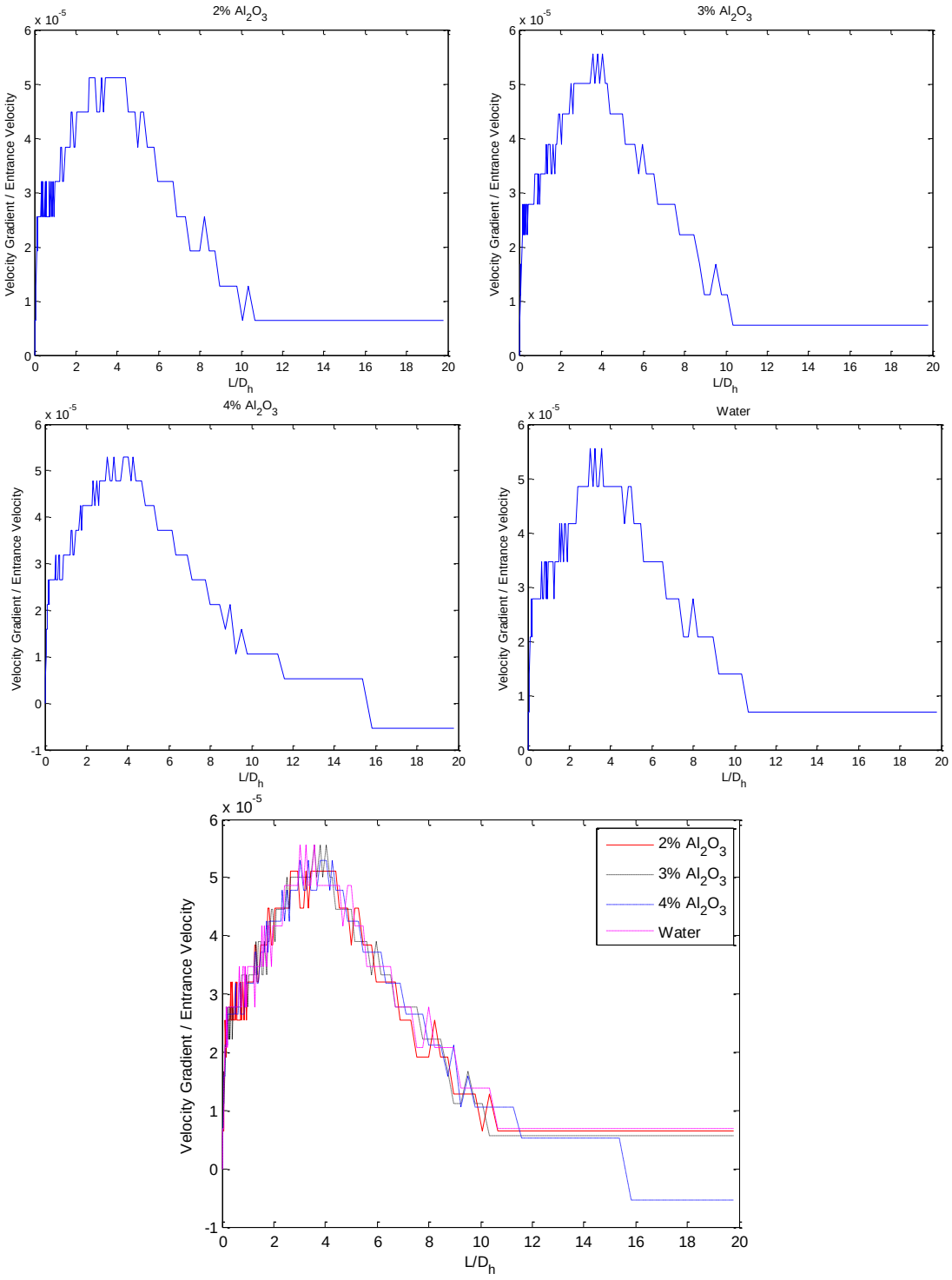

Figure 5.15 The normalized velocity gradient profile of water and Al2O3 nanofluids for turbulent channel flow at Re = 30000 using the k - ε turbulence model

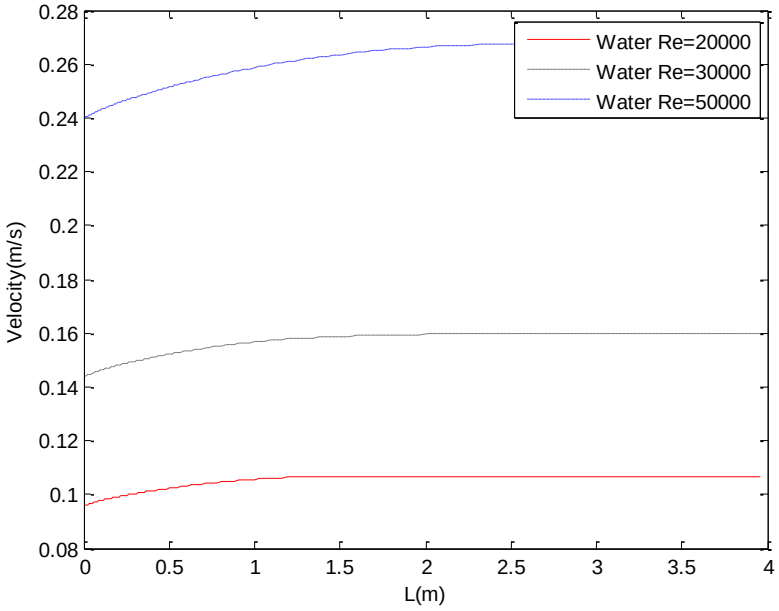

Figure 5.16 Centerline velocity profile of water and Al_2O_3 nanofluids for turbulent channel flow at Re = 20000, 30000, 50000 using the k - ε turbulence model

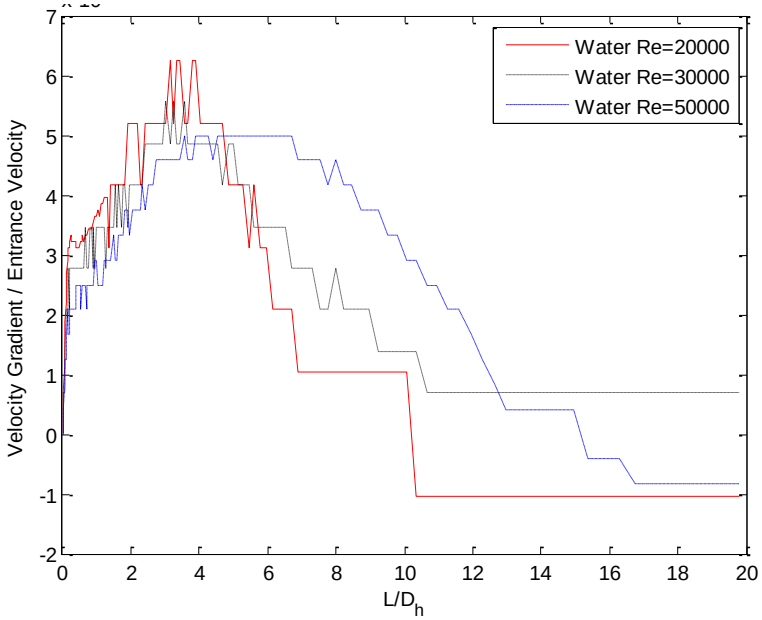

Figure 5.17 The normalized velocity gradient profile of water at different Reynolds numbers for turbulent channel flow using the k - ε turbulence model

Table 5.2 The dimensionless entrance length (L_h) of turbulent channel flow of water and Al_2O_3 nanofluids at Re = 30000 using the $k-\varepsilon$ turbulence model

Working Fluid	% of centerline velocity compared to fully developed value		
	99%	99.5%	99.9%
2%Al_2O_3	6.49985	7.9669	10.5113
3%Al_2O_3	6.49985	7.9669	10.5113
4%Al_2O_3	6.49985	7.9669	10.5113
Water	6.5254	8.021	10.6725

Table 5.3 The dimensionless entrance length L_h for turbulent channel flow at different Reynolds numbers using the $k-\varepsilon$ turbulence model

Reynolds number	% of centerline velocity compared to fully developed value		
	99%	99.5%	99.9%
20000	4.819365	5.51135	6.449
30000	6.5254	8.021	10.6725
50000	8.32875	9.59135	11.18105

5.3.3 Entrance Length Analysis using SST $k-\omega$ Model

Figure 5.18 shows the comparison of different turbulence models at Re = 30000 in a two dimensional channel flow. SST model, SA model, $k-\varepsilon$ model and $k-\omega$ model are employed. The same inlet turbulence boundary condition is used; the turbulent intensity is 4.41% and the hydraulic diameter is 0.2m. It can be seen that different turbulence models give different results on the same mesh with the same boundary conditions for the centerline velocity profile of the turbulent channel flow.

In Figure 5.18 (a), for SST k- ω model B, we employed a high inlet turbulent viscosity ratio and turbulent intensity value to promote immediate transition to turbulence. The turbulent viscosity ratio is 1000 and the turbulent intensity is 20%. The entrance length of the turbulent channel flow at Reynolds number ranging from 10000 to 60000 is calculated with the data obtained by numerical computations using SST k- ω model with high inlet turbulent viscosity ratio and high turbulent intensity. Figure 5.18 (b) shows the skin friction on the surface of one of the channel plates using different turbulence models. This figure shows that with the exception of k - ε model, all other turbulence model indicate a dip in the skin friction coefficient profile before it acquires the fully developed turbulent flow value. It demonstrates that the skin friction goes through a transition region from laminar value near the inlet of the channel to a fully turbulent value downstream. None of the models can capture this region accurately. It requires consideration of a more suitable transitional model.

The results of dimensionless entrance length L_h for different Reynolds numbers are shown in Table 5.4. It can be seen that, for centerline velocity to be 99.9% of the fully developed value, the L_h increases with increase in Reynolds number as expected. To obtain an equation for turbulent channel flow with new modified coefficients, the classical model for turbulent pipe flow is used.

$$\frac{L_e}{D} = x\,\mathrm{Re}^{y} \tag{5-10}$$

We consider all possible combinations of (*x, y*) pair in the range [0, 50] for *x* and [0, 1] for *y* and find that (10.41, 0.075) is the point that minimizes the square of the error, which is calculated by the following equation.

$$\frac{\sum_{i\in E}\left(l_h(i) - x\,\mathrm{Re}(i)^{y}\right)^2}{n} \tag{5-11}$$

where E is the set of experimental data and n is the size of E.

In this manner, the following equation to estimate the entrance length for turbulent channel flow is obtained.

$$\frac{L_e}{D} = 10.41\,\mathrm{Re}^{0.075} \tag{5-12}$$

As shown in Figure 5.19, the red curve is plotted with the new modified coefficients in Equation (5-12), and it is in good agreement with the computational data.

Table 5.4 The dimensionless entrance length (L_h) for turbulent channel flow at different Reynolds numbers using the SST turbulence model

Reynolds number	% of centerline velocity compared to fully developed value		
	99%	99.50%	99.90%
10000	14.6187	16.9227	20.54455
15000	14.81605	17.3219	21.3988
20000	14.96945	17.62235	22.00065
25000	15.06215	17.80125	22.3957
30000	15.1087	17.9455	22.685
35000	15.1398	18.01805	22.9325
40000	15.1398	18.09085	23.1368
45000	15.1398	18.1456	23.2969
50000	15.12425	18.1639	23.41185
55000	15.0932	18.1639	23.48105
60000	15.06215	18.1822	23.57365

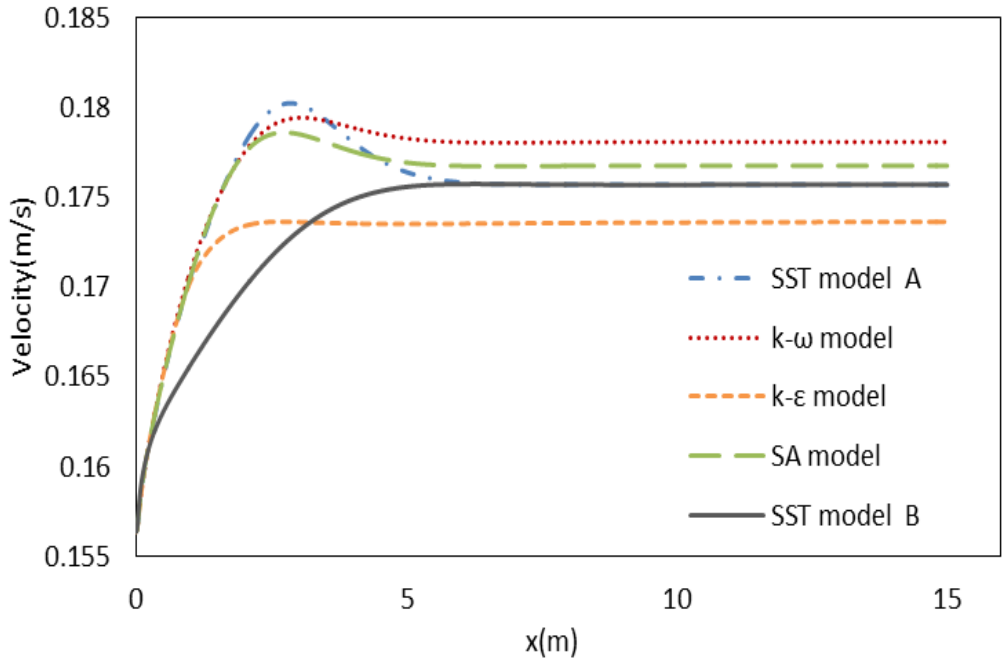

Figure5.18 (a) Comparison of centerline velocity using different turbulence models at Re = 30000 for 2D channel flow

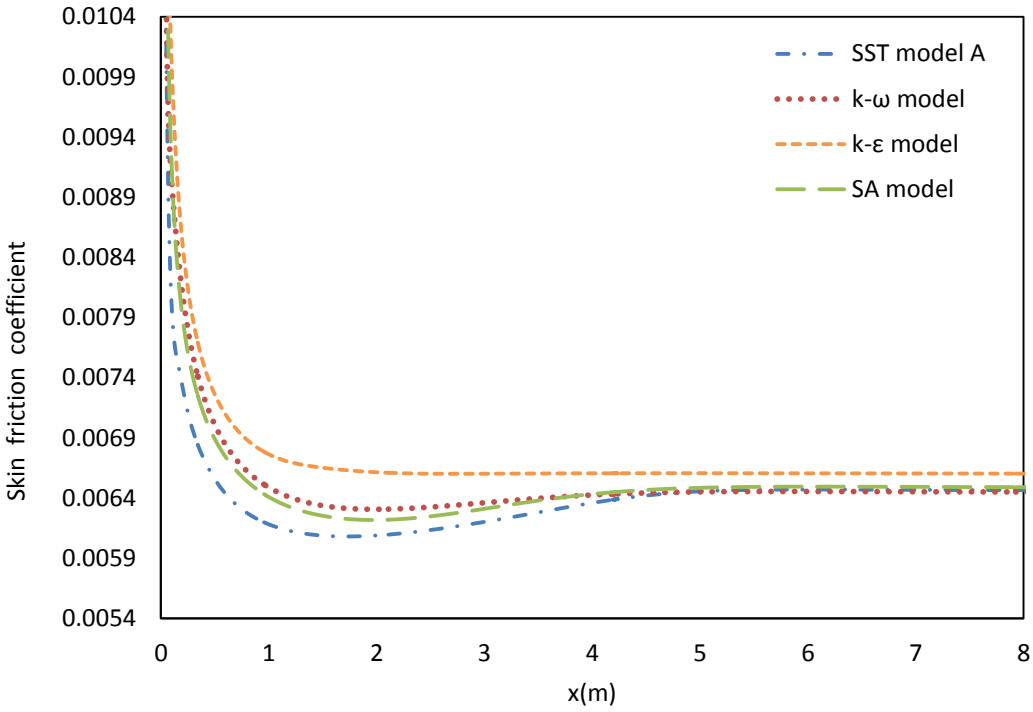

Figure5.18 (b) Comparison of skin-friction using different turbulence models at Re = 30000 for 2D channel flow

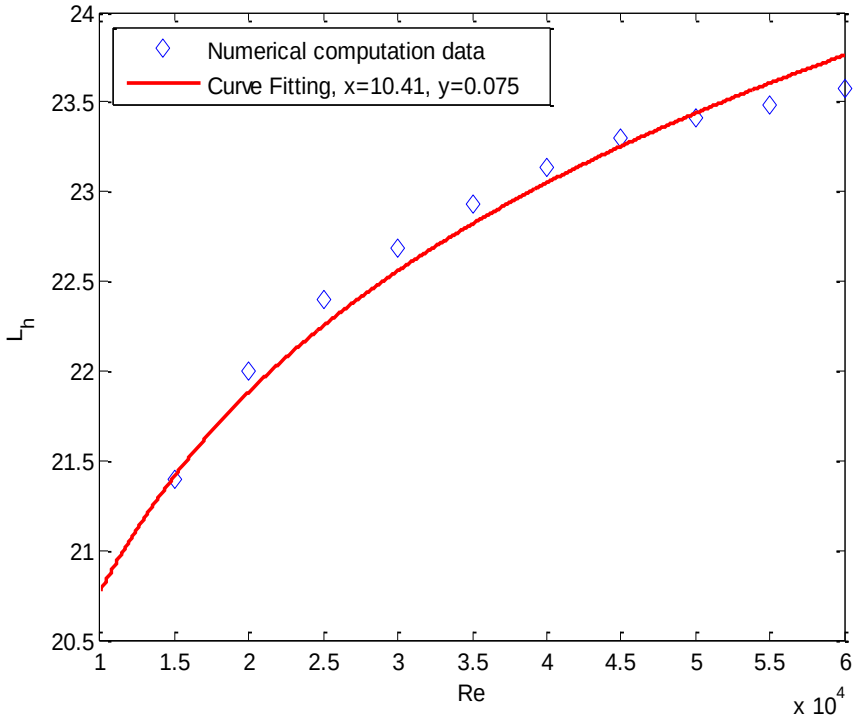

Figure 5.19 Comparison of the dimensionless entrance length L_h using equation (5-12) and the computational data at different Reynolds numbers

5.3.4 The Effect of Nanoparticle Concentration

Figure 5.20 shows the effect of nanoparticle volume fraction on the heat transfer coefficient in thermal entrance region of turbulent channel flow. Water and Al_2O_3/water nanofluids are used as working fluids. Pure water shows the lowest heat transfer coefficient. It is clear that the heat transfer coefficient increases with increase in nanoparticle concentration. Figure 5.21 illustrates the effect of nanoparticle volume fraction on the local Nusselt number at Reynolds number Re=30000. It shows the same trend as the heat transfer coefficient. Al_2O_3/water nanofluid shows the highest Nusselt number, which is caused by the high thermal conductivity. The average Nusselt number of 3%Al_2O_3/water nanofluids increases by 4.84% compared to that of pure water.

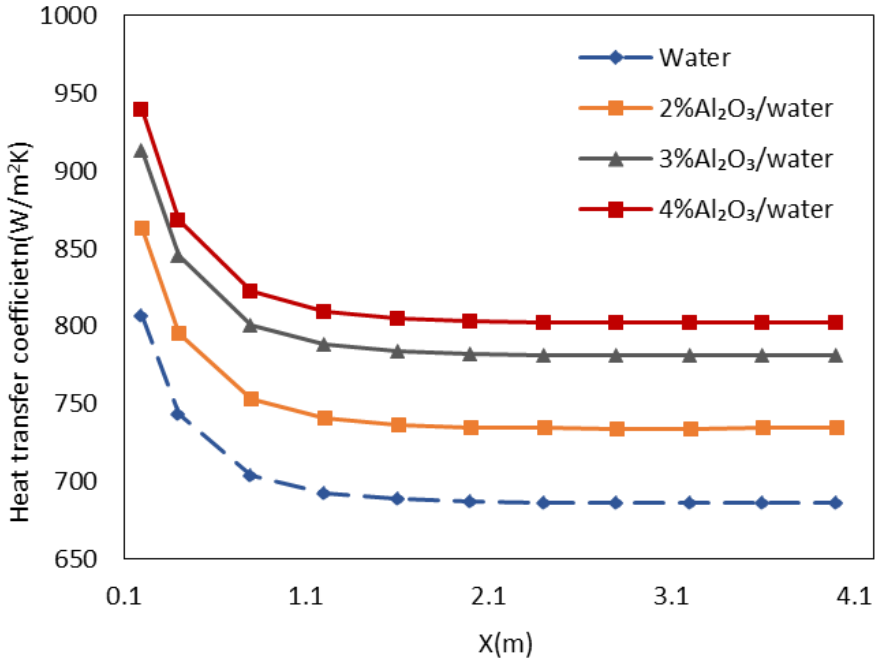

Figure 5.20 Axial variation of heat transfer coefficient for different particle volume concentrations of Al_2O_3/water nanofluid in turbulent channel flow at Re = 30000 using the k - ε turbulence model

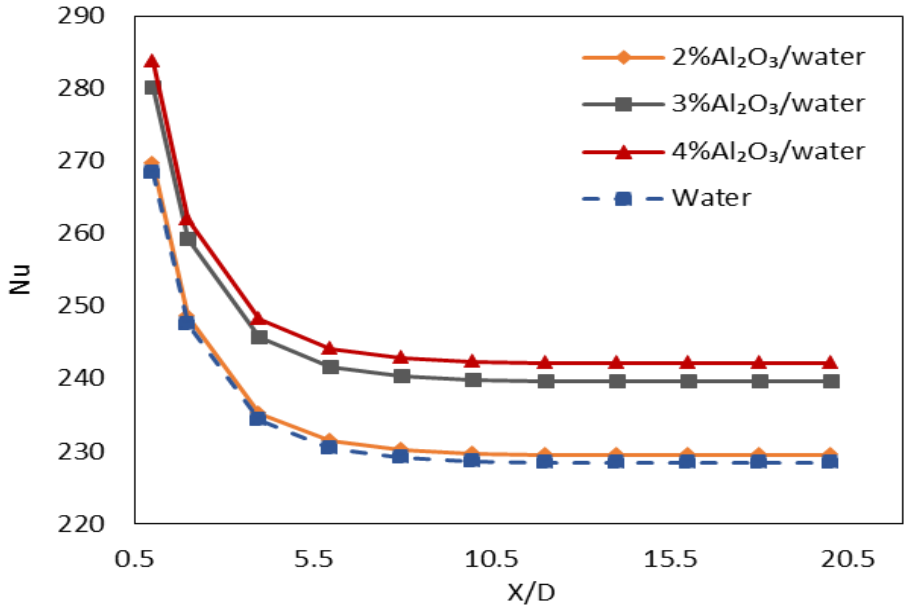

Figure 5.21 Axial variation of Nusselt number for different particle volume concentrations of Al_2O_3/water nanofluid in turbulent channel flow at Re = 30000 using the k - ε turbulence model

5.3.5 The Effect of Reynolds Number

Figure 5.22 shows the variation in the average Nusselt number as a function of Reynolds number for various volume fractions of Al_2O_3/water nanofluids. For all the studied volume fractions, the Nusselt number increases with increase in the Reynolds number. This is because of the improvement in heat transfer at higher Reynolds number. The other reason of this increase in average Nusselt number is due to increase in Brownian motion inside the nanofluids at higher Reynolds numbers, which results in a more uniform temperature distribution inside the flow field. Hence, the heat transfer rate between the nanofluid and wall increases.

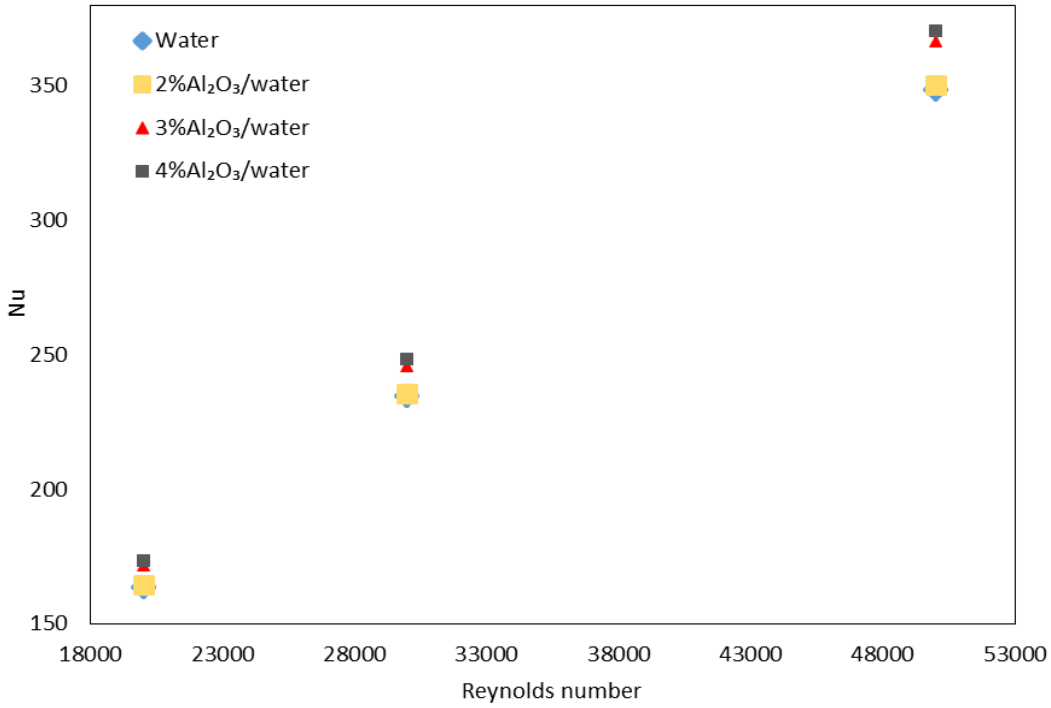

Figure 5.18 The variation of the average Nusselt number with Reynolds number for various volume fractions of nanofluids using the k - ε turbulence model.

5.3.6 The Effect of Nanoparticle Material

In order to study the effect of nanoparticle materials of turbulent channel flow; pure water, Al_2O_3/water and CuO nanofluids with volume fraction 2% and 4% are investigated at Reynolds number of 30000. In Figures 5.23 and 5.24, it can be seen that CuO/water nanofluids give higher heat transfer coefficient and Nusselt number than the Al_2O_3 nanofluids at the same nanoparticle concentration because of their higher thermal conductivity.

For CuO/water nanofluids with 2% and 4% nanoparticle concentration, the average Nusselt number increases by 5.45% and 17.95% compared to that for pure water, respectively. The average heat transfer coefficient of CuO/water nanofluids with 2% and 4% nanoparticle concentrations increases by 12.47% and 30.34% compared to that for pure water, respectively. This phenomenon indicates that CuO/water nanofluids show strong influence on the convective heat transfer enhancement.

CNT/water nanofluids with small particle concentrations show a significantly higher heat transfer enhancement compared to that with the other three nanofluids. For CNT/water nanofluids of 0.038% particle volume fraction, the average heat transfer increases by 50.95% and the average Nusselt number increases by 43.887% compared to that for pure water, respectively.

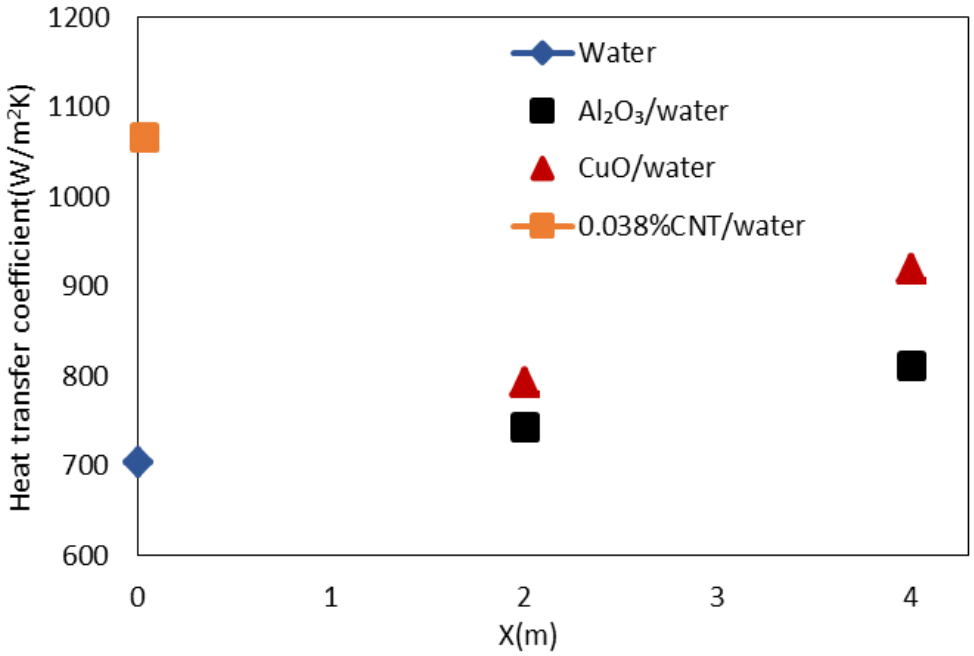

Figure 5.19 Effects of particle type and particle concentration on the average heat transfer coefficient for turbulent channel flow at Re = 30000 using the k - ε turbulence model

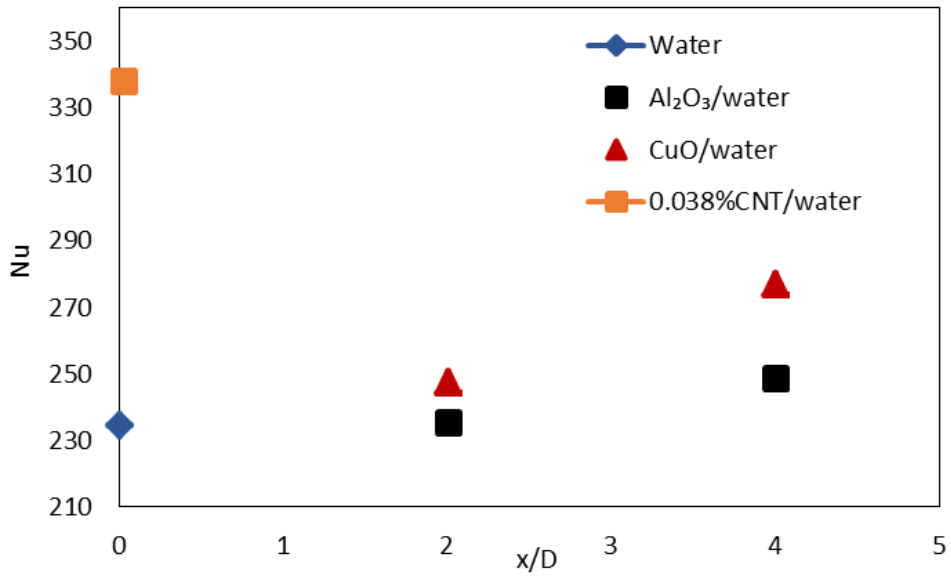

Figure 5.20 Effects of particle type and particle concentration on the average Nusselt number for turbulent channel flow at Re = 30000 using the k - ε turbulence model

Chapter 6 Conclusions

In this thesis, we have investigated the problems of fluid flow and heat transfer of nanofluids in pipe flow under constant heat flux boundary conditions and 2D channel flow under constant wall temperature boundary conditions, for both laminar and turbulent flow Reynolds numbers. The entrance length for both pipe and channel flow is also computed and compared with the available correlations in the literature. For turbulent flow simulations, two-equation k-epsilon, standard *k*-omega and SST *k*-omega models as well as the one-equation Spalart-Allmaras models are employed. Four new correlations with modified coefficients are obtained based on the numerical research presented in this thesis. Nanofluids show better heat transfer properties compared to pure water, and the increase in nanoparticles concentration increases the heat transfer coefficient and Nusselt number for all cases considered. CuO/water nanofluids show more influence on convective heat transfer compared to Al_2O_3 nanofluids because of the higher thermal conductivity of CuO compared to Al_2O_3. Finally, 0.038% CNT/water nanofluids significantly increase the heat transfer coefficient and Nusselt number in the flow field.

References

[1] S. U. S. Choi, and J. A. Eastman. "Enhancing thermal conductivity of fluids with nanoparticles." ASME-Publications-Fed, no. 231 (1995): 99-106.

[2] D. Wen, G. Lin, S. Vafaei, and K. Zhang. "Review of nanofluids for heat transfer applications." Particuology 7, no. 2 (2009): 141-150.

[3] M. Hidetoshi, A. Ebata, and K. Teramae. "Alteration of thermal conductivity and viscosity of liquid by dispersing ultra-fine particles. Dispersion of Al_2O_3, SiO_2 and TiO_2 ultra-fine particles." (1993): 227-233.

[4] S. Lee, S. U. S. Choi, S, and Li, and J. A. Eastman. "Measuring thermal conductivity of fluids containing oxide nanoparticles." Journal of Heat Transfer 121, no. 2 (1999): 280-289.

[5] Y. Xuan, and Q. Li. "Heat transfer enhancement of nanofluids." International Journal of Heat and Fluid Flow 21, no. 1 (2000): 58-64.

[6] Y. Xuan, and W. Roetzel. "Conceptions for heat transfer correlation of nanofluids." International Journal of heat and Mass transfer 43, no. 19 (2000): 3701-3707.

[7] J. A. Eastman, S. U. S. Choi, S. Li, L. J. Thompson, and S. Lee. "Enhanced thermal conductivity through the development of nanofluids." InMRS proceedings, vol. 457, p. 3. Cambridge University Press, 1996.

[8] R. Saidur, K. Y. Leong, and H. A. Mohammad. "A review on applications and challenges of nanofluids." Renewable and Sustainable Energy Reviews 15, no. 3 (2011): 1646-1668.

[9] S. Kakac, and A. Pramuanjaroenkij. "Review of convective heat transfer enhancement with nanofluids." International Journal of Heat and Mass Transfer 52, no. 13 (2009): 3187-3196.

[10] P. Tongpun, E. Bumrungthaichaichan, and S. Wattananusorn. "Investigation of entrance length in circular and noncircular conduits by computational fluid dynamics simulation." Songklanakarin Journal of Science and Technology 36, no. 4 (2014): 471-475.

[11] G. K. Batchelor. "An introduction to fluid dynamics." Cambridge University Press, Third Edition, 2000.

[12] S. P. Jang, and S. U. S. Choi. "Role of Brownian motion in the enhanced thermal conductivity of nanofluids." Applied physics letters 84, no. 21 (2004): 4316-4318.

[13] J. Koo, and C. Kleinstreuer. "A new thermal conductivity model for nanofluids." Journal of Nanoparticle Research 6, no. 6 (2004): 577-588.

[14] R. Prasher, P. Bhattacharya, and P. E. Phelan. "Thermal conductivity of nanoscale colloidal solutions (nanofluids)." Physical review letters 94, no. 2 (2005): 025901.

[15] D. H. Kumar, H. E. Patel, V. R. Kumar, T. Sundararajan, T. Pradeep, and S. K. Das. "Model for heat conduction in nanofluids." Physical Review Letters 93, no. 14 (2004): 144301.

[16] H. E. Patel, T. Sundararajan, and S. K. Das. "A cell model approach for thermal conductivity of nanofluids." Journal of Nanoparticle Research 10, no. 1 (2008): 87-97.

[17] J. Lee, S. Lee, C. Choi, S. Jang, and S. U. S. Choi. "A review of thermal conductivity data, mechanisms and models for nanofluids." International Journal of Micro-Nano Scale Transport 1, no. 4 (2010): 269-322.

[18] C. Pang, W. L. Jae, H. Hong, and Y. T. Kang. "Heat conduction mechanism in nanofluids." Journal of Mechanical Science and Technology 28, no. 7 (2014): 2925-2936.

[19] P. Keblinski, S. R. Phillpot, S. U. S. Choi, and J. A. Eastman. "Mechanisms of heat flow in suspensions of nano-sized particles (nanofluids)." International journal of heat and mass transfer 45, no. 4 (2002): 855-863.

[20] R. Prasher, P. E. Phelan, and P. Bhattacharya. "Effect of aggregation kinetics on the thermal conductivity of nanoscale colloidal solutions (nanofluid)." Nano Letters 6, no. 7 (2006): 1529-1534.

[21] J. W. Gao, R. T. Zheng, H. Ohtani, D. S. Zhu, and G. Chen. "Experimental investigation of heat conduction mechanisms in nanofluids. Clue on clustering." Nano letters 9, no. 12 (2009): 4128-4132.

[22] W. Evans, P. Ravi, F. Jacob, P. Meakin, P. Phelan, and P. Keblinski. "Effect of aggregation and interfacial thermal resistance on thermal conductivity of nanocomposites and colloidal nanofluids." International Journal of Heat and Mass Transfer 51, no. 5 (2008): 1431-1438.

[23] W. Yu, and S. U. S. Choi. "The role of interfacial layers in the enhanced thermal conductivity of nanofluids: a renovated Maxwell model." Journal of Nanoparticle Research 5, no. 1-2 (2003): 167-171.

[24] J. S. Maxwell. A treatise on electricity and magnetism. Vol. 1. Clarendon press, 1881.

[25] R. L. Hamilton, and O. K. Crosser. "Thermal conductivity of heterogeneous two-component systems." Industrial & Engineering chemistry fundamentals 1, no. 3 (1962): 187-191.

[26] C. H. Chon, K. D. Kihm, S. P. Lee, and S. U. S. Choi. "Empirical correlation finding the role of temperature and particle size for nanofluid (Al_2O_3) thermal conductivity enhancement." Applied Physics Letters 87, no. 15 (2005): 153107-153107.

[27] S. P. Jang, and S. U. S. Choi. "Effects of various parameters on nanofluid thermal conductivity." Journal of Heat Transfer 129, no. 5 (2007): 617-623.

[28] J. Koo, and C. Kleinstreuer. "Viscous dissipation effects in microtubes and microchannels." International Journal of Heat and Mass Transfer 47, no. 14 (2004): 3159-3169.

[29] R. Prasher, P. Bhattacharya, and P. E. Phelan. "Thermal conductivity of nanoscale colloidal solutions (nanofluids)." Physical review letters 94, no. 2 (2005): 025901.

[30] Y. Xuan, Q. Li, X. Zhang, and M. Fujii. "Stochastic thermal transport of nanoparticle suspensions." Journal of applied physics 100, no. 4 (2006): 043507.

[31] J. Li. "Computational Analysis of Nanofluid Flow in Microchannels with Applications to Micro-heat Sinks and Bio-MEMS. " PhD thesis, North Carolina State University, 2008.

[32] A. Einstein. "Investigations on the Theory of the Brownian Movement." Courier Corporation, 1956.

[33] H. C. Brinkman. "The viscosity of concentrated suspensions and solutions." The Journal of Chemical Physics 20, no. 4 (1952): 571-571.

[34] Y. Xuan, Q. Li, and W. Hu. "Aggregation structure and thermal conductivity of nanofluids." AIChE Journal 49, no. 4 (2003): 1038-1043.

[35] Q. Xue, and W. Xu. "A model of thermal conductivity of nanofluids with interfacial shells." Materials Chemistry and Physics 90, no. 2 (2005): 298-301.

[36] T. L. Bergman, F. P. Incropera, and A. S. Lavine. "Fundamentals of heat and mass transfer." John Wiley & Sons, Seventh Edition, 2011.

[37] Y. Xuan, and W. Roetzel. "Conceptions for heat transfer correlation of nanofluids." International Journal of heat and Mass transfer 43, no. 19 (2000): 3701-3707.

[38] B. C. Pak, and Y. I. Cho. "Hydrodynamic and heat transfer study of dispersed fluids with submicron metallic oxide particles." Experimental Heat Transfer an International Journal 11, no. 2 (1998): 151-170.

[39] Q. Li, and Y. Xuan. "Convective heat transfer and flow characteristics of Cu-water nanofluid." Science in China Series E: Technological Science 45, no. 4 (2002): 408-416.

[40] Y. Xuan, and Q. Li. "Investigation on convective heat transfer and flow features of nanofluids." Journal of Heat transfer 125, no. 1 (2003): 151-155.

[41] R. S. Vajjha, D. K. Das, and D. P. Kulkarni. "Development of new correlations for convective heat transfer and friction factor in turbulent regime for nanofluids." International Journal of Heat and Mass Transfer 53, no. 21 (2010): 4607-4618.

[42] J. Koo, and C. Kleinstreuer. "Laminar nanofluid flow in microheat-sinks." International Journal of Heat and Mass Transfer 48, no. 13 (2005): 2652-2661.

[43] S. E. Haaland. "Simple and explicit formulas for the friction factor in turbulent pipe flow." Journal of Fluids Engineering 105, no. 1 (1983): 89-90.

[44] W. Duangthongsuk, and S. Wongwises. "An experimental study on the heat transfer performance and pressure drop of TiO_2-water nanofluids flowing under a turbulent flow regime." International Journal of Heat and Mass Transfer 53, no. 1 (2010): 334-344.

[45] ANSYS Inc., ANSYS user manual.

[46] X. Chen. "Optimization of Wind Turbine Airfoils/Blades and Wind Farm Layouts." PhD thesis , Washtington University in St. Louis, 2014.

[47] M. Izadi, A. Behzadmehr, and D. Jalali-Vahida. "Numerical study of developing laminar forced convection of a nanofluid in an annulus." International journal of thermal sciences 48, no.11 (2009): 2119-2129.

[48] D. Kim, Y. Kwon, Y. Cho, C. Li, S. Cheong, Y. Hwang, J. Lee, D. Hong, and S. Moon. "Convective heat transfer characteristics of nanofluids under laminar and turbulent flow conditions." Current Applied Physics 9, no. 2 (2009): e119-e123.

[49] A. J. Chamkha, and E. Abu-Nada. "Mixed convection flow in single-and double-lid driven square cavities filled with water–Al_2O_3 nanofluid: Effect of viscosity models." European Journal of Mechanics-B/Fluids 36 (2012): 82-96.

[50] R. S. Vajjha, D. K. Das, and D. R. Ray. "Development of new correlations for the Nusselt number and the friction factor under turbulent flow of nanofluids in flat tubes." International Journal of Heat and Mass Transfer 80 (2015): 353-367.

[51] Y. He, Y. Men, X. Liu, H. Lu, H. Chen and Y. Ding. "Study on forced convective heat transfer of non-Newtonian nanofluids." Journal of Thermal Science 18, no. 1 (2009): 20-26.

[52] M. Corcione. "Heat transfer features of buoyancy-driven nanofluids inside rectangular enclosures differentially heated at the sidewalls." International Journal of Thermal Sciences 49, no. 9 (2010): 1536-1546.

[53] S. K. Das, N. Putra, P. Thiesen, and W. Roetzel. "Temperature dependence of thermal conductivity enhancement for nanofluids." Journal of Heat Transfer 125, no. 4 (2003): 567-574.

[54] P. Keblinski, S. R. Phillpot, S. U. S. Choi, and J. A. Eastman. "Mechanisms of heat flow in suspensions of nano-sized particles (nanofluids)." International journal of heat and mass transfer 45, no. 4 (2002): 855-863.

[55] B. B. Munson, D. F. Young, and T. H. Okiishi. "Fundamentals of fluid mechanics." New York, 1990.

[56] S. G. Etemad. PhD Thesis, McGill University, 1995.

[57] J. P. D. Plessis, and M. R. Collins. "A new definition for laminar flow entrance lengths of straight ducts." N&O Joernaal 25 (1992): 11-16.

[58] A. Aghaei, G. A. Sheikhzadeh, M. Dastmalchi, and H. Forozande. "Numerical investigation of turbulent forced-convective heat transfer of Al_2O_3–water nanofluid with variable properties in tube." Ain Shams Engineering Journal (2015).

[59] A. Bijan. "Convection heat transfer." John Wiley & Sons, Third Edition, 1984.

[60] G. Roy, I. Gherasim, F. Nadeau, G. Poitras, C. T. Nguyen. "Heat transfer performance and hydrodynamic behavior of turbulent nanofluid radial flows." International Journal of Thermal Sciences 58 (2012): 120-129.

[61] A. Kruskopf, T. Siikonen and R. Agarwal. "Application of multigrid methods for solution of incompressible Navier-Stokes equations using a pressure-correction algorithm." 2015.

[62] F M. White. "Viscous Fluid Flow." McGraw-Hill International Edition, Third Edition, 2006.

Vita

Yihe Huang

Degrees M.S Mechanical Engineering, Washington University in St. Louis, August 2015

B.S Material Science and Engineering, Harbin Institute of Technology, July 2013